Production and Characterization of Novel Flow Battery Electrodes via Electrospinning

Selina (Peng) Liu

Chemical Engineering

McGill University, Montreal

June, 2017

A thesis submitted to

McGill University in partial fulfillment of the

requirements of the degree of Master of Engineering

Table of Contents

Table of Figures and Tables

Abstract

Large scale energy storage is necessary in deploying more renewable but intermittent electricity sources into our electricity grid. Even though the redox flow battery is a promising technology, its limited performance and high costs are major barriers to mass adoption in the market. Optimizing electrode properties has been shown to be a promising avenue to improve performance. Rather than modifying commercially available carbon paper, this work focused on fabricating novel materials via electrospinning followed by carbonization. Materials with fiber diameter of around 900 nm and porosity of more than 85% were produced. This material was characterized before and after carbonization for fiber diameter, porosity, in-plane permeability and pore size distribution. Conductivity and surface area were also measured for the carbonized fibrous material. It was found that fiber diameter and porosity decreases during carbonization. However, this does not affect the permeability, which is caused by a change in the morphology of the mat. This thesis has successfully fabricated suitable material for flow battery testing. With the detailed characterization results, we are one step closer to understanding the effect of electrode properties on redox flow battery cell performance.

Abstrait

Un stockage d'énergie à grande échelle est nécessaire pour développer des sources d'électricité renouvelables intermittentes dans notre réseau électrique. Même si la batterie à flux est une technologie prometteuse, ses performances limitées et ses coûts élevés sont des obstacles majeurs à son adoption sur le marché. L'optimisation des propriétés des électrodes est une avenue prometteuse pour améliorer la performance de ces batteries. Plutôt que de modifier le papier carbone disponible sur le marché, ce travail qui suit traite de la fabrication de nouveaux matériaux par électrofilage combiné à la carbonisation. Des matériaux ayant un diamètre de fibre d'environ 900 nm et une porosité de plus de 85% ont été produits. Ce matériau a été caractérisé avant et après la carbonisation pour mesurer le diamètre de la fibre, la porosité, la perméabilité dans le plan et la distribution de la taille des pores. La conductivité et la surface ont également été mesurées pour le matériau fibreux carbonisé. Il a été constaté que le diamètre et la porosité de la fibre diminuent pendant la carbonisation. Cependant, cela n'affecte pas la perméabilité, qui est causée par une modification de la morphologie de échantillon. Cette thèse fait état du succès de la fabrication des matériaux appropriés pour le test de la batterie à flux. Par l'obtention de résultats caractérisation détaillés, nous sommes plus près de la compréhension de l'effet des propriétés de l'électrode sur la performance des cellules de la batterie à flux.

Acknowledgements

I would like to first acknowledge the entire Porous Material Engineering and Analysis Lab (PMEAL), led by Professor Gostick. I have learned a lot from Jeff in the last several years from doing an undergraduate research project to doing this master's thesis. Jeff is an inspiration in being curious and determined to expand scientific knowledge. I need to especially thank Matt Kok who has done so much in helping me understand what I've been doing every day, and to have kept me sane in the office. Matt provided a tremendous amount of help in designing, building and troubleshooting all the experimental setups. Many thanks to other lab members: Yongwook Kim for all the speedy experiments you ran for me, Jon Unno for patiently showing me how the stress-strain machine works, Shaqa for all the delicious treats, Amin Sadeghi and Mahmoud Aghighi for all the interesting conversation. I'd like to thank the Plasma group, especially Larissa Jorge, for teaching me and allowing me to use the tube furnace. Thanks to Jonathan Verrett for providing editing help, and Julie Ducharme for providing French translation help for the abstract.

I'd also like to acknowledge all the staff in the WONG building, including all the technicians (Frank Caporuscio, Lou Cusmich, Gerald Lepkyj, Andrew Golstajn, Ranjan Roy, and Monique Riendeau) and the administrative staff (Louise Miller, Jo-Ann Gadsby and Lisa Volpato).

Lastly I'd like to acknowledge my funding sources: Department of Chemical Engineering for the Eugene Ulmer Lamothe award and the Natural Sciences and Engineering Research Council of Canada for the CSG Award.

Preface and Contribution of Authors

In this thesis; BET surface area results were measured by Monique Riendeau, a Mining & Materials Engineering technician. The electrospinning experiment set up was done in collaboration with Matt Kok. Design of porosity, permeability and thickness had been previously developed by members of PMEAL. All other work was done by the author, Selina Liu.

1. Introduction and Literature review

As our society starts to move away from fossil fuel based energy sources, more renewable energy will be integrated to our energy system. According to the Renewable Energy Policy Network for 21st Century (REN21), renewable energy (not including hydroelectricity) made up 10.3% of the total amount of energy produced in 2014 around the world, and 23.7% of the total electricity production in 2015 [1]. Of this, 3.7% and 1.2% is made up of wind and solar respectively [1]. These amounts may seem low for now, but the cost of these technologies have been rapidly decreasing, rendering them more and more competitive. Solar and wind have grown at a remarkable rate of 42% and 17% between 2010 to 2015 respectively [1]. This rapid growth can be problematic, however, since both solar and wind produce intermittent power, meaning that the production of electricity is not constant and does not necessarily match the demand of power. As the deployment of these types of electricity generation increase, they pose a threat to the current electricity grid, causing instabilities and possible blackouts. Energy storage is an essential requirement to bridge the gap between intermittent supply and variable demand [2]. Other applications of energy storage technologies include levelling demand peaks during the day, storing surplus energy production during the night to meet demand during the day, and reducing the need for stand-by energy production plants based on natural gas. Not only is energy storage important in ensuring the stability and efficiency of the grid, but it can also reduce the cost of electricity for the consumer [3].

Many ways to store energy are in development; an overview of the current technology will be discussed in the background section of this thesis. Redox flow batteries have been

identified as a favorable large scale energy storage option [4]. This thesis explores the potential to increase performance of redox flow batteries by optimizing electrode properties. The remainder of this section will first provide a background on the redox flow battery. The importance of electrode materials and their characteristics will then be discussed. An opportunity to redesign and fabricate material via Electrospinning will then explored further. Section 2 provides more detailed background information on energy storage technologies, the current state of flow battery research, and material fabrication techniques. Section 3 outlines methods used in this thesis for generating and characterizing materials used. Section 4 presents and discusses the result from the experiments. Lastly, lessons learnt, future work and conclusions are discussed.

1.1. Flow Batteries

Redox flow batteries are a promising option due to their decoupled energy and power capacity, geographic and chemical flexibility and ease of scale-up [2], [4]. Electricity is stored in the form of chemical potential energy while redox reactions allow the cell to be charged and discharged. A typical configuration can be seen in Figure 1.

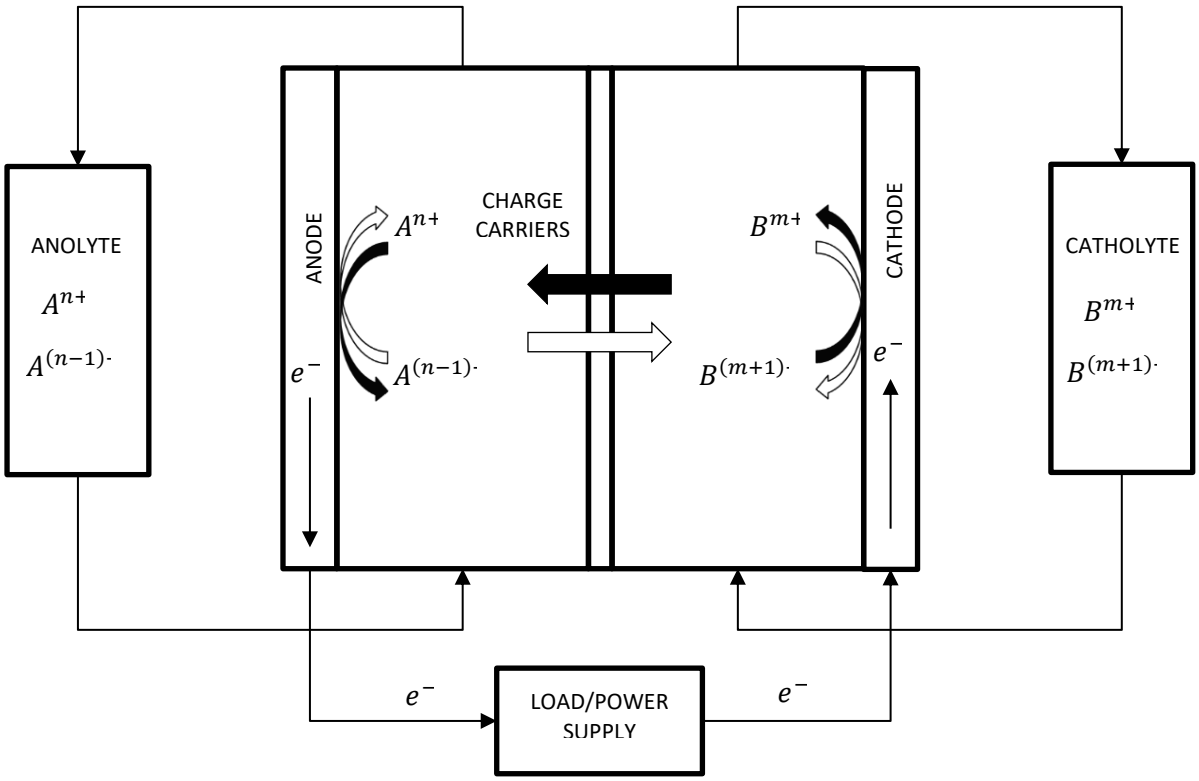

Figure 1 Typical Schematic of a Redox Flow Battery

During discharge, anolyte is pumped to the anode from an external tank; it then reacts on the surface of the electrode to release electrons which flow through an external circuit, to the load. The charge carrier species, such as H^+, travels across the Ion Exchange Membrane, which is aimed at separating the anolyte from the catholyte. The following hypothetical reactions occur within a generic flow battery:

$$A^{n+} + xe^- \xrightarrow{charge} A^{(n-x)+}; \quad A^{(n-x)+} \xrightarrow{discharge} A^{n+} + xe^-$$

$$B^{m+} \xrightarrow{charge} B^{(m+y)+} + ye^-; \quad B^{(m+y)+} + ye^- \xrightarrow{discharge} B^{m+}$$

The primary advantage of a flow battery is the decoupled energy and power, allowing for greater flexibility in integrating flow batteries in different applications. The energy storage capacity is determined by the size of tanks holding the electrolyte solutions. The larger the tank, the more

energy the system can store. These are separate from the reactive cell which determines the power of the system. The power of the cell is denoted by kW or MW. A watt can be broken down to voltage multiplied by current. The voltage of the system is dictated by the redox chemistry combinations and their standard voltage potential. Each cell operates at a certain voltage, and multiple ones can be stacked on top of one another to achieve higher voltages [2]. Many researchers focus on finding reactants that are more cost effective [5], or would yield higher voltages [6]. A brief overview of this field of research can be found in the background section of this thesis. The chemistry of the flow battery technology is not the focus of this thesis, and the presented findings can be applied to any chemical system.

Power density is commonly used as a measurement of cell performance. Another method to improve the efficiency or performance of the cell is to increase the current density, [A/cm2]. This can decrease the cell size while achieving the same current which will decrease the cost of the technology and lead to higher economic feasibility. Figure 2 is a generic polarization curve that demonstrates possible losses that occurs in a typical flow battery set up. Three main types of losses include activation, ohmic and transport. This thesis focuses on reducing the transport losses within the electrode.

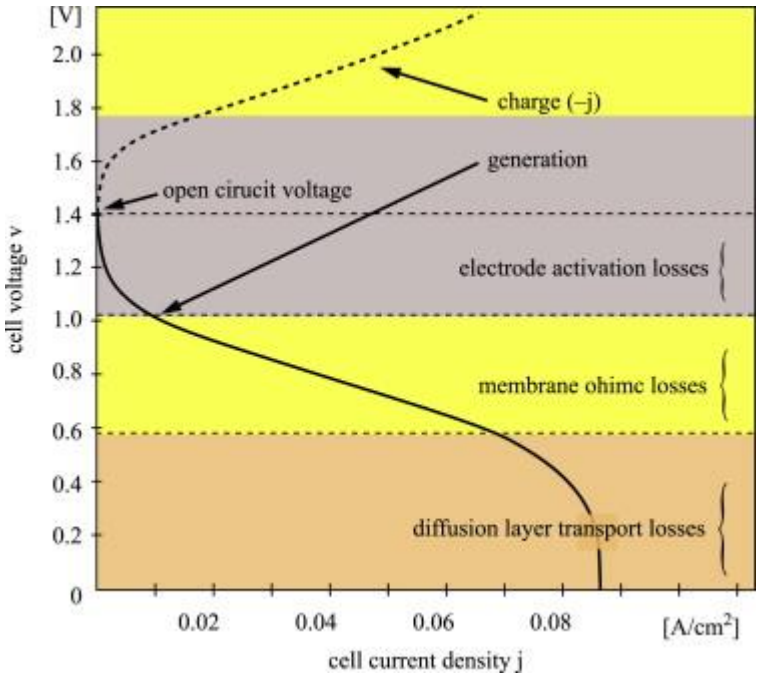

Figure 2 Potential losses of a redox flow battery [2]

When electrolyte is pumped to the electrochemical cell, chemical reactions occur within the electrode, at the solid-liquid interface. To achieve higher reaction rates, and therefore higher power density, the electrodes need to have high active surface area, but must also have good mass transport properties so the reactants can fully utilize the area. Flow channels bring the reactant to the electrode, which can be seen in Figure 3 a). Figure 3 b) demonstrates some possible configurations. The electrode would be placed on top of the flow channel for all cases except the flow through configuration in which the electrode is placed inside the flow channel. The reactant flow in perpendicular direction to the plane of the flow field. For example, the reactant in an interdigitated flow field is forced to flow through the electrode. In addition, flow batteries can also be operated by flowing the reactive liquid past a flat graphite plate. The interdigitated flow field pattern has shown to yield the highest performance [7].

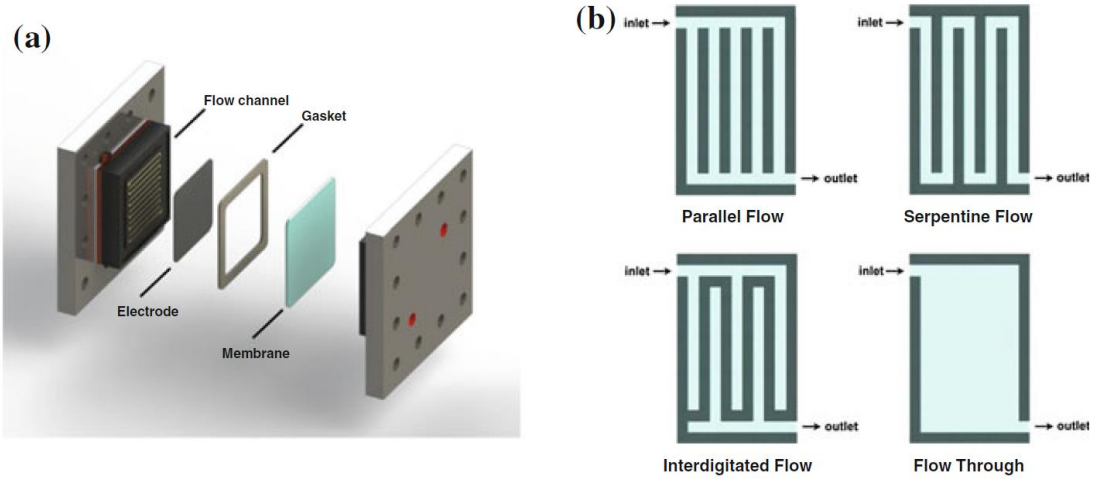

Figure 3 a) Component view of a redox flow battery cell, b) different flow channel configurations [6] The electrode is on top of the flow channels. The reactants also flow perpendicular to the plan of the flow field.

Currently, the most commonly used material for porous electrodes is commercially available carbon-fiber paper used as the Gas Diffusion Layer (GDL) of a fuel cell. Some common brands include SGL 25AA, Toray 90 and Freudenberg. These types of GDL will be discussed and compared in section 4. Attempts to increase performance of these carbon papers have included stacking multiple layers [8]–[10], laser etching holes [11], growing carbon nanotubes on fiber surfaces [12], [13] and thermal activation [14]. An alternative approach, which is explored in this thesis, is to increase the volumetric current density by making a fibrous electrode with much smaller fibers and therefore more specific surface area.

1.2. Fibrous Material

Fibrous materials offer several key properties that make them ideally suited for electrodes. This section will discuss the effect of fiber diameter and porosity, two essential characteristics, on properties such as surface area and permeability. As a first approximation, the specific surface

area, A_s, (m^2/m^3) of a fibrous material can be estimated by assuming that all of the solid in the bulk volume is a continuous filament of diameter d_f. The length, L, of this filament is based on the solid volume which can be determined from the mass of the mat, m, and the skeletal density of the solid, ρ_s:

$$L = \frac{V_s}{A_C} = \frac{m\rho_s}{\frac{\pi}{4}d_f^2} \quad \textbf{(1)}$$

The specific surface area of this single fictitious filament is then found from:

$$A_s = \frac{\pi d_f L}{V_b} \quad \textbf{(2)}$$

where V_b is the bulk volume of the mat. Eq. (2) can be simplified by inserting Eq.(1) for L and noting that the solid volume V_S can be expressed $V_b(1-\varepsilon)$:

$$A_s = \frac{4(1-\varepsilon)}{d_f} \quad \textbf{(3)}$$

where $\epsilon = \frac{V_{pore}}{V_{bulk}}$ is the porosity of the material. It provides a useful estimate about the interplay between fiber size and the porosity of the mat. Specifically, smaller fibers and lower porosity lead to more specific surface area since these both mean more fibers per unit volume.

Improving cell performance is not as straightforward as using a tightly packed array of smaller fibers however. The permeability coefficient, K, of the mat must also be considered since it controls how easily liquid reactant flows through the electrode. Similar to traditional porous material such as beds of sand and rocks, electrolyte flow through the electrode is governed by Darcy's law

$$Q = \frac{KA}{\mu L}\Delta P \quad \textbf{(4)}$$

where Q is the volumetric flow rate of the fluid (m^3/s), A is the cross-sectional area of the fluid

flow (m^2), μ is the viscosity of the fluid (Pa·s), ΔP is the pressure drop (Pa) across length L (m). Darcy's law shows that for a given pressure a higher K will result in higher reactant flow rates, leading to higher interstitial velocity, and better mass transfer between the bulk and fiber surface. For a fibrous material, its permeability coefficient is well characterized by the Carmen-Kozeny equation [15]–[17]

$$K = \frac{d_f^2 \varepsilon^3}{16 k_{ck} (1-\varepsilon)^2} \quad \textbf{(5)}$$

The value k_{ck} is a fitting parameter, which accounts for the material structure other than porosity and fiber diameter, such as fiber morphology and shape. For example, granular porous materials have different k_{ck} from fibrous material, and aligned fibrous material have different k_{ck} value from randomly aligned fibers. Eq. (5) shows that the permeability coefficient decreases sharply with decreasing fiber size and porosity, which means that efforts to increase surface area per Eq. (5) will be at the expense of flow properties of the electrode. This can be clearly seen in Figure 4 where equation 1 and 3 are plotted against each other.

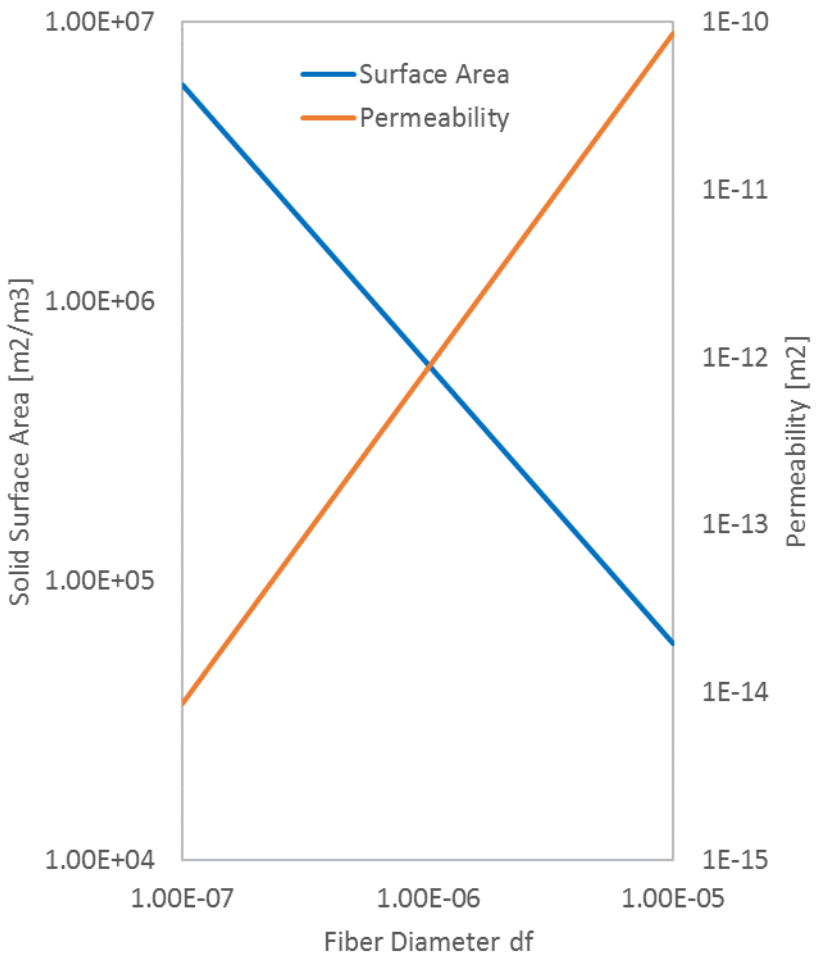

Figure 4 Theoretical surface area and permeability properties for an 85% porous fibrous material

The competition between specific surface area and permeability creates an optimization problem to find the values of porosity and fiber diameter that will result in the best overall cell performance. Recently, Kok *et al.* used multi-physics modeling to study the effect of various physical properties of fibrous electrodes on transport properties and performance of a flow battery [18], with the aim of predicting optimal properties. The results showed that the optimal arrangement is a fiber diameter around 1 to 2 µm coupled with a high porosity above 85%. This is much different than the commercially available materials which have fiber diameter around 10

μm and porosity below 75% [19].

1.3. Fabricating Novel Electrodes via Electrospinning

With the above information at hand, it is feasible to produce actual materials with these optimized parameters for practical testing. Electrospinning is a useful technique for producing prototype fibrous materials with the desired characteristics. Electrospinning can utilize a wide variety of polymeric materials and easily control the fibrous morphology, therefore creating a wide range of advanced materials for applications such as filtration, sensing, and tissue engineering [20]. A more detailed overview of electrospinning, its theories and applications can be found in the background section. For the use of an electrode in flow cells, the material needs to conduct electricity, provide a reactive surface, and be durable in the harsh acidic environment of the flow cell, so this limits the choice to a polymer that can be carbonized. Polyacrylonitrile (PAN) was chosen since it is an excellent material for carbon fiber precursor [21] due to its high carbon yield [21]. In addition, electrospinning PAN has been well researched and optimized [22], [23]. However, the literature in the carbonization of PAN is focused on the production of carbon fiber [21], [24], and less for other applications. Further discussion of these studies along with a more detailed description of the carbonization steps are provided in the Chapter 2. Even though there's extensive knowledge in the chemical and physical property transition during carbonization [25], there's a lack of information on the effect of carbonization on transport properties of electrospun material. In addition, electrospinning of carbon fiber favors small fibers, the reported fiber diameter is usually less than 300 nm [26], [27], which is well below the range of optimized fiber diameter [18].

Several review papers [28]–[30] have specifically summarized the applications of electrospun carbon fiber mats in various energy storage applications, including super capacitors, fuel cells, and Li-ion batteries [31], [32], but less attention has been directed towards flow batteries. Two groups have explored and tested electrospun electrodes in a flow battery [33], [34], but they focused specifically on the impact of carbonization and surface chemistry on the reaction kinetics of vanadium for all-vanadium cells. To date, no study has been done to optimize cell performance by modifying the material structure to enhance transport properties. It is essential to be able to characterize these important properties to understand their effect on the performance of the flow battery. This thesis explores the potential of making better electrodes for flow batteries, including investigating ideal electrospinning conditions to produce desired materials, defining optimal carbonization conditions, and characterizing electrospun mats before and after carbonization, by looking at all the key transport properties including material thickness, fiber diameter, porosity, electrical conductivity, and permeability.

2. Background

This chapter provides detailed discussion on the energy storage technologies, other research in flow batteries, electrospinning and carbonization of PAN.

2.1. Overview of Energy Storage Technologies

Flow batteries store electrical energy in the form of chemical potential energy, however electrical energy can also be stored in other forms. Hydroelectricity or pumped hydro stores electricity in the form of potential energy. Electricity is used to pump water uphill and stores energy. Then, when water flows downhill, electricity can be generated. The power capacity and discharge time are two crucial factors that determine the applicability of an energy storage technology. Figure 5 demonstrates the range of different technologies and their applications. Along with pumped hydro, compressed air energy storage (CAES) is another example for bulk power management. In other words, they are suitable for storing a large amount of energy, but take a long time to discharge the energy. In a CAES system, electricity is stored when compressing air in an underground cavern; when the electricity is needed, the air is heated, which then decompresses, turning a turbine to produce electricity [35]. An American company, LightSail for example, is pursuing this technology further. On the opposite end of the spectrum to bulk power, high power supercapacitors and high power flywheels are suitable for applications with short discharge time. In electric or hybrid vehicles, super capacitors are used in conjunction with batteries or fuel cells to recuperate energy via regenerative braking and to provide quick bursts of power for acceleration [31], [36].

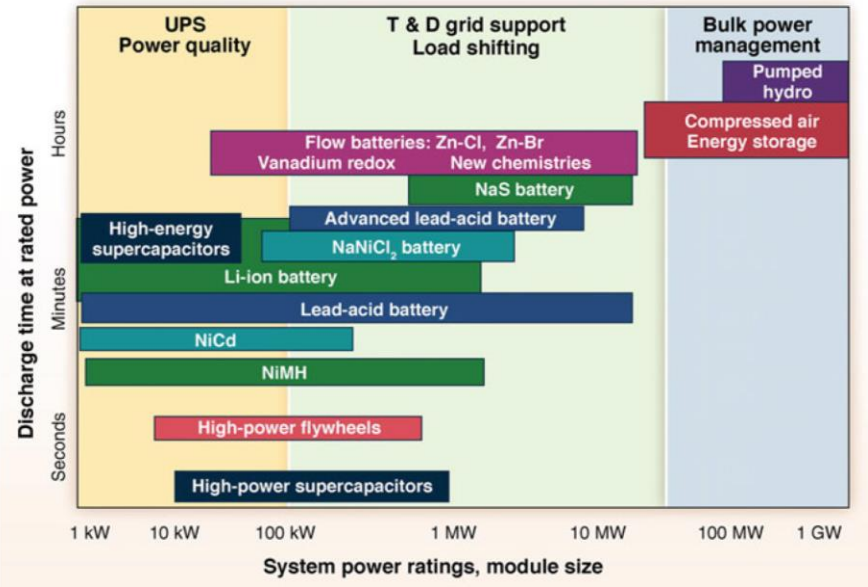

Figure 5 Overview of current energy storage technologies [6]

Between these two extremes of the spectrum, there are many battery technologies with discharge time ranging from minutes to hours, with capacity sizes from 1kW to 10MW. Flow batteries cover a large range of capacity size for longer discharge time applications. Li-ion batteries, a more commercially adopted technology, usually have smaller capacity and discharge quicker compared to that of flow batteries. Li-ion batteries are commonly used in personal portable electronic devices, and electrical vehicles [37]. As the name implies, Li-ion batteries rely on Li, an expensive material that needs to be mined. The high cost of material is a major barrier for large scale energy storage.

2.2. Flow Battery Chemistries

As mentioned above, flow battery comes in a wide range of capacity and discharge time. One reason is the endless possibility in its redox chemistry. Different chemistry combination results in different reaction time, and electric potential, resulting in a wide range of results.

Finding alternative redox chemistries for flow batteries is an active field of research. As mentioned in the introduction, this can reduce the cost of the total system, and/or increase the redox potential or voltage of the system. Redox potential depends on the standard redox potential which is the difference between the two standard potentials of the redox reactions that occur at the electrodes. Increasing redox potential can increase the power density of the cell. Currently, the all-Vanadium redox (VRB) chemistry is among the most commercially developed technology [38], [39], with several pilot projects installed [38]. The electrochemical reactions involved are the following:

Positive Electrode:	$VO_2^+ + 2H^+ + e^- \Leftrightarrow VO^{2+} + H_20$	E^o=+0.991V
Negative Electrode:	$V^{3+} + e^- \Leftrightarrow V^{2+}$	E^o=-0.255V
Total Reaction:	$VO_2^+ + V^{2+} + 2H^+ \Leftrightarrow VO^{2+} + V^{3+} + H_20$	E^o=1.246V

Sulfuric acid is typically used as the supporting electrolyte to increase ionic conductivity. Despite progress in the field, VRB has yet to see mass commercialization, some main challenges include its low energy density (<25 Wh/L) [6] due to the low solubility of $VOSO_4$, the high cost of Vanadium and toxicity of Vanadium. Other aqueous metallic, or inorganic-aqueous chemistry couples include iron-chromium, polysulfide-bromide [2], [4]. In 2014, researchers at Harvard made a significant breakthrough using organic-aqueous species, quinone/hydroquinone with a Br_2/Br^- redox couple to achieve a power density of 0.6W/cm^2 [5]. Quinone is a type of organic species, and the 9,10-anthraquinone-2,7-disulphonic acid (AQDS) is the specific molecules used. This nontoxic chemistry can dramatically decrease the cost of electrolyte [5] since it contains no costly metals such as vanadium. Further research is conducted in replacing the Br_2/Br^- redox couple with a quinone type species to create a fully organic flow battery.

Nonaqueous systems have recently gained interest due to higher cell voltage windows (they can span greater than 4V) and higher ion solubility. This leads to higher energy density and possibly higher efficiencies [6], [40]. Metal-centered coordination complexes such as $Ru(bpy)_3$ with acetonitrile as the solvent and $TEABF_4$ as the supporting salt have cell voltages of 2.6V [41]. A molecular diagram of $Ru(bpy)_3$ is shown in Figure 6. The challenges of these systems are the higher cost of the non-aqueous solvents and major safety concerns due to their flammability [6].

Figure 6 Molecular diagram of $Ru(bpy)_3$ [6]

Hybrid flow batteries are defined as when one of the redox couples is either a metal or a gas. This include Zn-air, technology being developed by companies such as FluidicEnergy and ZincNyx. Hydrogen bromine is another potential chemistry that has recently gained a lot of attention in the US [9]. The reactions and its standard potential can be seen below.

Positive Electrode:	$Br_{2(aq)} + 2e^- \Leftrightarrow 2Br_{aq}^-$	E^o=+1.098V
Negative Electrode:	$H_{2(g)} \Leftrightarrow 2H^+ + 2e^-$	E^o=0V
Total Reaction:	$H_{2(g)} + Br_{2(aq)} \Leftrightarrow 2HBr_{(aq)}$	E^o=1.098V

As shown in the above reactions, liquid bromine is at the cathode and hydrogen gas is at the anode. This phase difference means species crossover is not an issue. In addition, bromine is readily available and less toxic compared to vanadium. The modelling done by Kok et al. is based on this chemistry, which provides the electrode properties guidelines for this thesis.

2.3. Electrospinning

Electrospinning is short for “electrostatic spinning” [20]. It is a prominent technique for prototyping fibrous material without the need for high temperature polymer melts. It uses electrostatic forces to stretch polymer molecules in a solvent solution into thin fibers. When polymer solution enters an electric potential field, typically created by a grounded collector and a needle charged with a high voltage, the potential field overcomes the surface tension of the polymer solution and shears the polymer as the solvent evaporates. Filaments are then formed. A theoretical set up is shown in Figure 7.

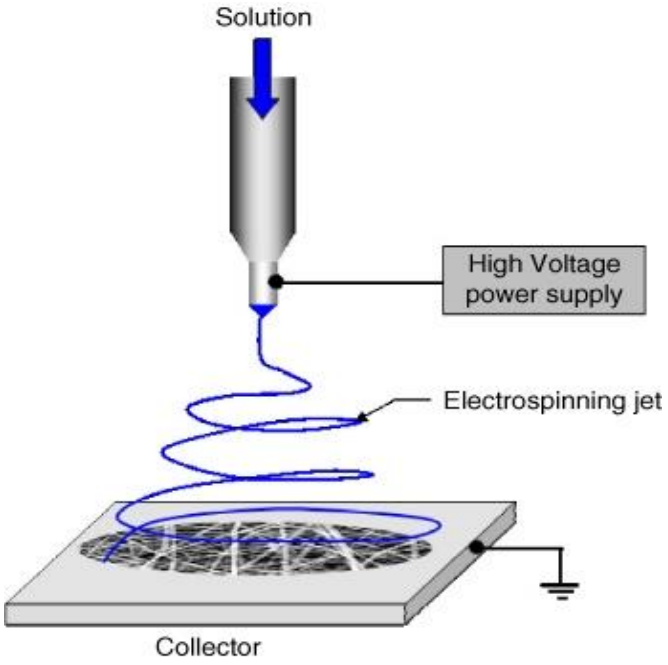

Figure 7 Hypothetical electrospinning set up

A variety of polymers can be electrospun, to create material with different applications. These materials range from commodity polymer such as polystyrene [42], to biocompatible polymer such as PCL [43], to biopolymer such as chitin from shrimp shells [44]. A combination of

polymers can be used such as PAN and PMMA. After carbonizing, PMMA melts away due to its lower melting point, and a microporous material is created [45]. Studies done for this thesis involved electrospinning a PAN solution dissolved in dimethylformamide (DMF). PAN was chosen due to its high carbon yield during the carbonization step [21], and for the extensive research done in the context of PAN electrospinning.

Many parameters can affect the morphology and properties of the final material. These include viscosity, conductivity, voltage difference, feed rate, spinneret tip-to-collector distance and humidity [46]. Increasing polymer concentration increases viscosity of the spin solution, which increases fiber diameter with a roughly linear relationship [47], [48]. Increasing applied voltage typically decreases the fiber diameter due to increased shearing [49]. When the spinneret tip-to-collector distance is too small, solvent does not have enough time to fully evaporate and spinning conditions are not stable [49].

The solution delivery system is not limited to an individual needle. Co-axial electrospinning allows tubular structured micro fibers, and core shell structures to be formed [50]. Different polymers can be used to form the core and shell. Needleless electrospinning has been shown to work [51], [52], and Elmarco, a company based in the Czech Republic is developing technology that is fabricating electrospun material on an industrial scale. Nor is the collector limited to a simple plate. For example, a rotating drum collector can be used to create a sheet of final material. A rotating drum was used for the work done in this thesis. Photos of the set up can be found in section 3. When the speed of rotation of the drum is very high, highly aligned fibers can be made which favors permeability in the direction of alignment [17].

In summary, electrospinning is an extremely versatile method in producing fibrous materials. By varying the material used to electrospin and/or the method to electrospin, material with desirable properties can be designed and created. This diversity in material property leads to applications ranging from water treatment to tissue engineering and to energy storage.

2.4. Carbonization of PAN

As this thesis studies the feasibility of producing flow battery electrode via electrospinning, one essential property of the electrode is electroconductivity. Carbonization transforms electrospun PAN material to conductive material. The molecular structure of PAN $[C_3H_3N]_n$ is shown in Figure 8.

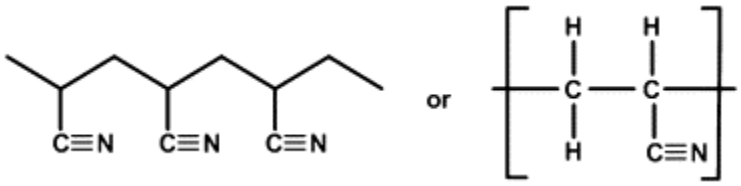

Figure 8 Molecular structure of polyacrylonitrile, PAN [53]

In the process of converting PAN to carbon fibers, the steps shown in Figure 10 are carried out. When using a carbonized mat for an electrode in a flow battery, the strength and purity of the material are not of high priority, the material only needs to be conductive enough. Therefore, the material only goes through the stabilization and carbonization steps. This requires lower temperatures than that of graphitization. During the stabilization step, the fibers are oxidized in air. Many chemical reactions occur in this step such as cyclization, dehydrogenation, aromatization, oxidation and crosslinking, which are shown in Figure 9. The triple bonds between carbon and nitrogen is converted to double bonds. Temperature is an important factor to ensure

complete stabilization, typically in the range of 180 – 300 °C. If the temperature is too low, the process will be too slow and may be incomplete, but if the temperature is too high, the fibers may fuse together or burn [53].

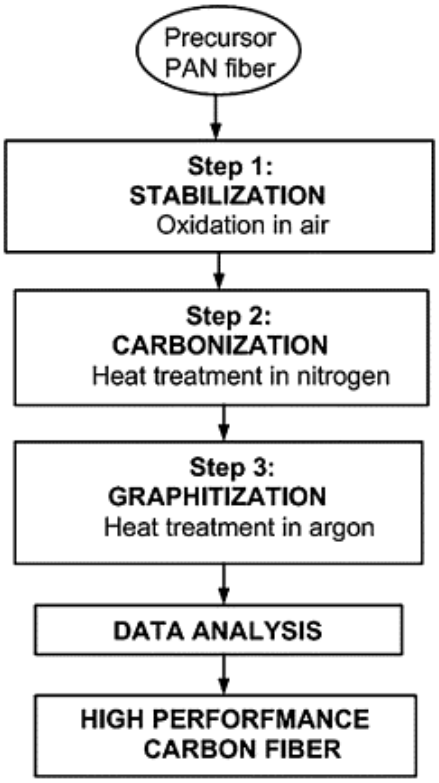

Figure 10 Steps in using PAN as a carbon fiber precursor [56]

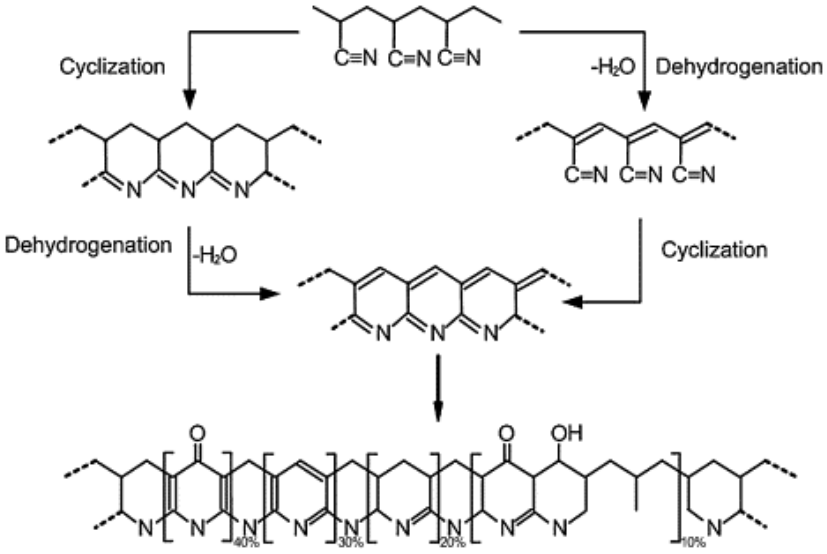

Figure 9 Chemical processes that occur during stabilization

The carbonization of PAN for the production of carbon fiber started in the 1960s [24]. It is now the most commonly used precursor to carbon fiber due to its high carbon yield (around 50%). The study of carbonization of PAN fibers is primarily focused on the production of carbon fiber, with the aim of producing stronger and smaller fibers. Even though researchers have used carbonized fibrous mats for other applications, such as in electrochemistry or filtration, minimal transport properties characterization have been done on these types of materials.

The above have provided background information on energy storage, flow battery

research, electrospinning technique and steps in PAN carbonization. It's been demonstrated that customized flow battery electrode with targeted material properties have not been thoroughly studied. This thesis aims to demonstrate the feasibility of producing flow battery electrode with targeted material properties derived from modelling studies. The material will be produced via electrospinning, followed by carbonization of PAN. Very little is known regarding the transition of electrospun mat and their transport properties. This thesis is aimed at addressing this knowledge gap through detailed characterization of both electrospun and carbonized electrospun material.

3. Experimental Methods

The electrospun mats were made using a custom-built setup, and then carbonized in an inert environment furnace to produce a carbonaceous electrode. Various properties were physical and transport properties were measured before and after carbonization. This section will first describe the material production process, followed by descriptions of the numerous characterization methods applied.

3.1. Material Production

3.1.1. Electrospinning

Electrospinning was performed with custom-built device consisting of a rotating drum of 4 in. (10cm) diameter, a syringe pump, and a high-voltage power supply. A linear motion actuator was used to raster the needle back and forth across the drum to increase the coating width and ensure an even deposition of fibers on the drum. Photos of the set up are shown in Figure 11. A negative-polarity power supply used with the negative terminal connected to the collector. Everything else was grounded to ensure safety. It was found that the polarity of the power supply was very important to the fiber sizes and stability of electrospinning. In a previous study, Ali et al. [54] found that fiber diameter was larger when the collector is charged rather than the needle, which is the most typical electrospinning configuration. Additionally, it was observed that by charging the collector with a negative voltage, the electrospinning process remained stable for a longer period of time, which was essential in producing samples with the required thickness.

Polyacrylonitrile (PAN) (Sigma, MW 150,000) was the chosen polymer due to its high

carbon yield. The spinning solution was prepared by dissolving PAN in N, N-dimethylformamide (DMF) (Sigma, anhydrous, 99.8%) to a varying composition between 10 and 13 wt%. Higher concentrations of the solution are known to increase the fiber diameter [55]. The solution was stirred for 20 hours without heating to ensure homogeneity without thermal degradation. All samples were electrospun with a 16 gauge (1.194 mm inner diameter) needle, 15kV applied voltage, a needle to collector distance of 15cm, collector rotation speed of 5 m/min (measured with a tachometer), and coating length of 6 in. (15 cm), and rastering speed of 5 mm/s. Flow rate was slowly decreased throughout spinning to maintain steady spinning conditions, from 0.8 mL/hr to 0.5 mL/hr. Each electrospun mat was made by spinning 30 mL of solution.

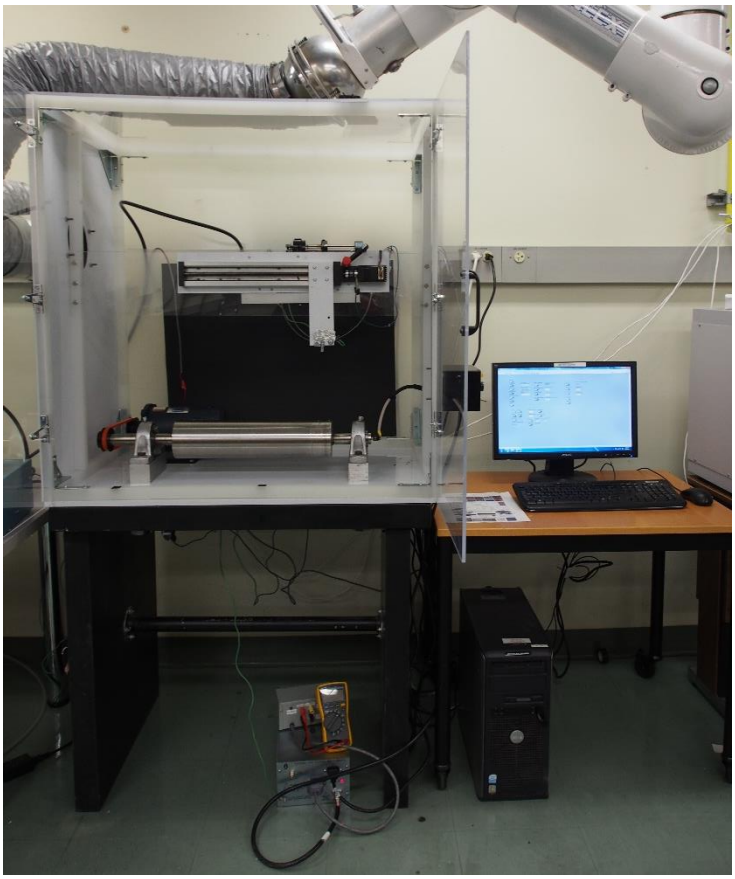

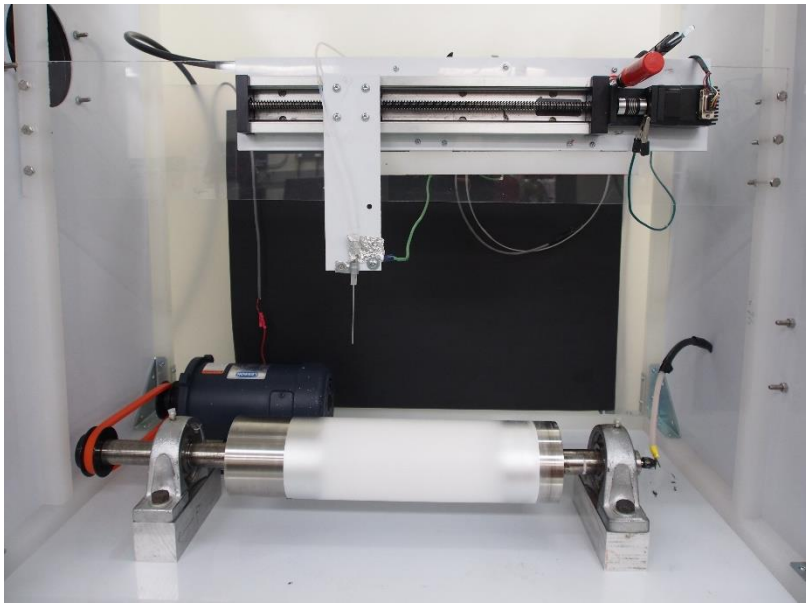

Figure 11 Photos of the electrospinner

3.1.2. Carbonization

Following electrospinning, the material was cut into pieces 5 by 20 cm and carbonized in a tube furnace, between two alumina plates approximately 1/8” (0.3175 cm) thick. A photo of the tube furnace is shown in Figure 12. The carbonizing of PAN fibers is a well-documented procedure, and typical conditions were used here [24], [26], [53]. The material was first stabilized in air, with a heating rate of 5°C/min and a plateau at 250°C for 75 minutes. Argon was introduced at 25 sccm after the sample has been stabilized for an hour. The temperature was continually increased at a rate of 5°C/min, plateauing at 850°C and 1050°C both for 40 minutes.

Figure 12 Tube furnace used for the carbonization step

3.2. Material Characterization

3.2.1. Fiber Diameter Determination

Fiber diameter, d_f, was obtained from scanning electron microscope (SEM) images (HITACHI 35000). These images were analyzed in ImageJ to estimate fiber diameter. Line segments were drawn across fibers and the length was taken as the width of fibers. SEM images were obtained from 5 different locations on each mat to ensure a representative range of values, and 30 measurements were taken from each image to get the average fiber diameter and the standard deviation.

3.2.2. Porosity Measurement

Porosity, ε, of the electrospun PAN mat was calculated by measuring the mass and volume of a sample cut by a hole punch with 3/8 in. diameter. Assuming that the electrospun fibers have the same density as PAN (1.184 g/cc), the mass of the sample was measured with an analytical balance with 0.0001 g resolution. The ratio of the mass to the PAN density gives the solid volume of the sample. Thickness is a delicate property to measure for highly porous and compressible electrospun mats. Thickness was measured with a force sensitive micrometer, as described by Kok et al. [17] A photo of the setup is shown in Figure 13. The sample is compressed until a 20 mN force had been applied, which was taken to be the boundary of the electrospun mat. With the known diameter and thickness, the total volume can be calculated. Taking the difference between the total and solid volumes gives the pore volume, which gives the porosity of the electrospun mat.

The porosity of the carbonized electrode could not be obtained with the above method since the density of the carbonaceous material was not well known. Instead, it was obtained using a buoyancy method shown to work well for measuring the porosity of thin fibrous media [19]. A photo of the setup is shown in Figure 14. Thickness of the carbonized electrode was measured with a micrometer equipped with a thumb clutch, with 1µm resolution and ±0.1µm accuracy. This was acceptable since the carbonized materials were notably stiffer. The sample was then weighed both dry and submerged in a wetting fluid such as silicone oil. Applying Archimedes principle allowed the determination of the solid or skeletal density, which can be used directly to find the solid volume fraction and then the porosity.

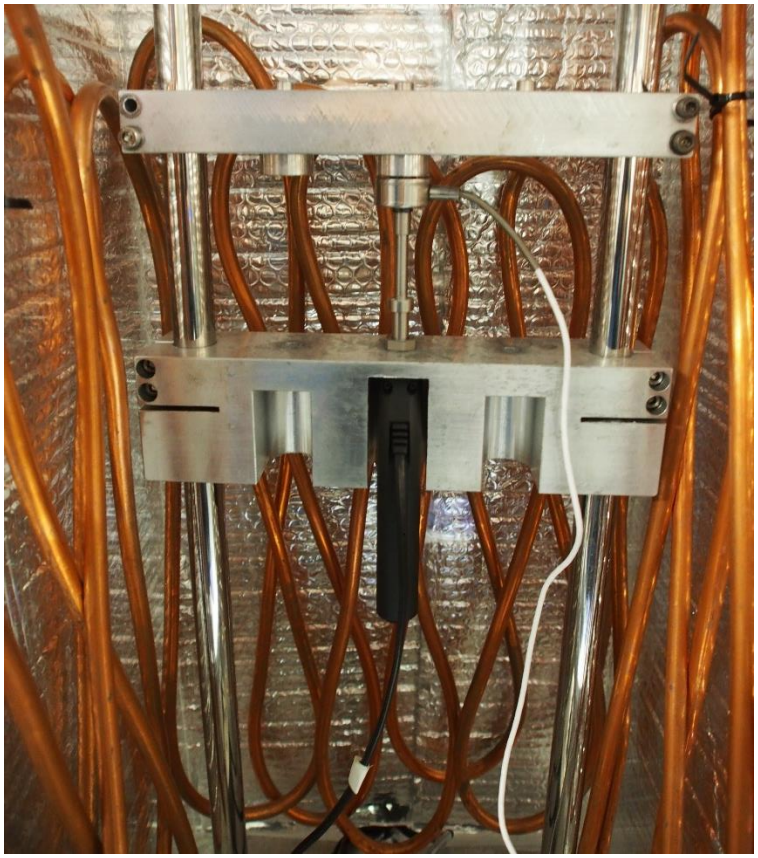

Figure 13 Stress-Strain device, used for thickness measurement

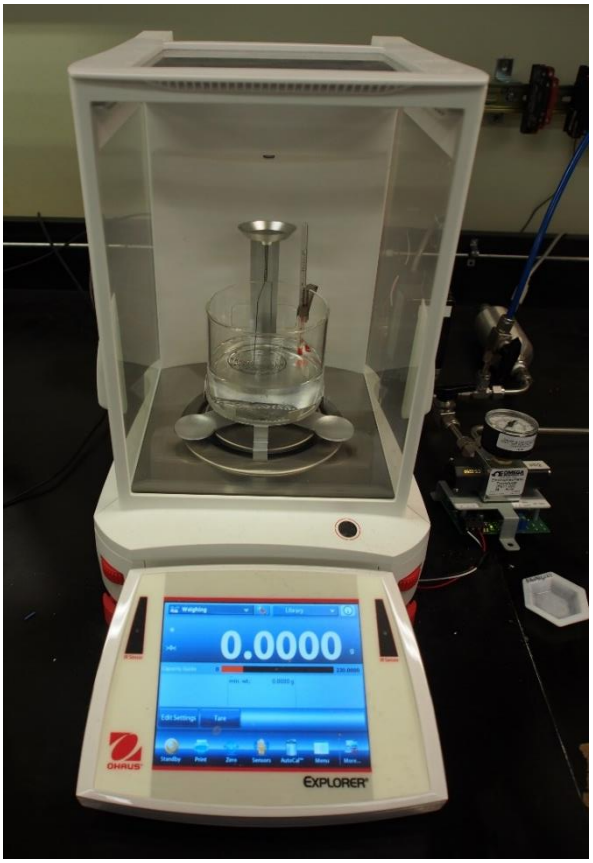

Figure 14 Porosity Measurement Set up

3.2.3. Surface Area

Specific surface area was measured using gas sorption analysis with a Micromeritics TriStar 3000, using nitrogen gas at 77K. Only the carbonized samples were tested for surface area since the degassing procedure involved heating to 120 °C, which would have damaged the PAN sample. The samples were cut into small square pieces, 0.5 cm wide, allowing them to fit in the testing tubes, and about 50 mg's were tested to ensure a detectable amount of surface area. Surface area was extracted from the isotherms using the standard Brunauer–Emmett–Teller (BET) theory.

3.2.4. Permeability

In-plane permeability, *K*, of the electrospun and carbonized materials were measured using a device and techniques developed by Gostick et al. [16] which was adapted for electrospun material by Kok et al. [17]. A photo of the setup is shown in Figure 15. Compressed air was supplied at the inlet by a mass flow controller (MKS 1160b series) with a range of 200 SCCM. Since the flowing fluid was compressible (i.e. air), the following version of Darcy's Law was used.

$$\frac{P_{in}^2 - P_{out}^2}{2LRT/MW_{air}} = \frac{\mu}{K} m' \qquad (6)$$

The flow rate did not exceed 100 SCCM to ensure that no Forchheimer effect was observed [16]. The inlet pressure was measured by a pressure sensor (Omega PX409, 0 – 30 psia range), and the outlet pressure was open to atmosphere which was taken from the inlet pressure sensor prior to flowing air and confirmed by comparing to the local weather station. A sample of 0.5" × 2" was cut and placed in the sample holder. Permeability was measured at varying degrees of

compression which was controlled by placing shims of known thickness between the plates prior to tightening them together.

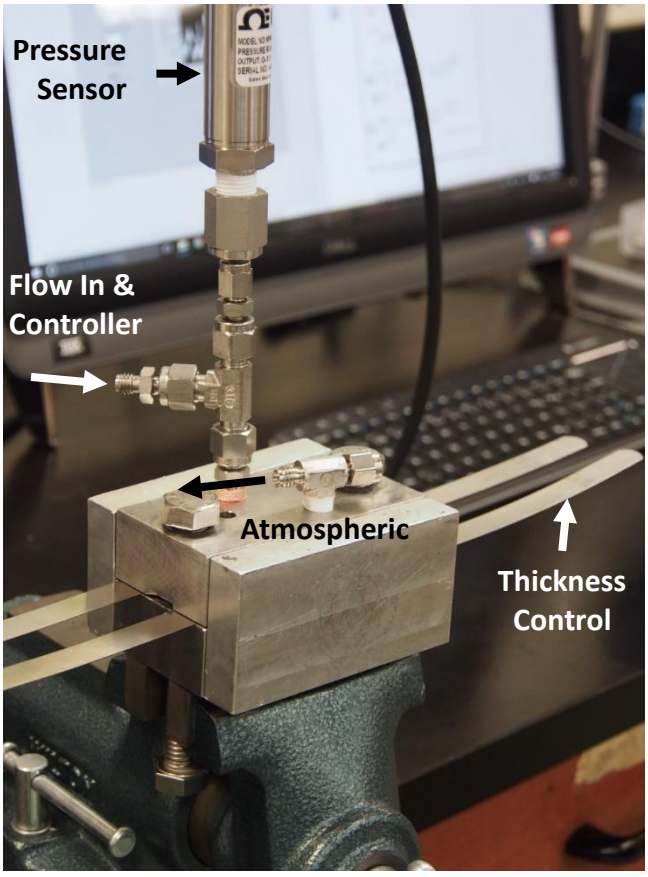

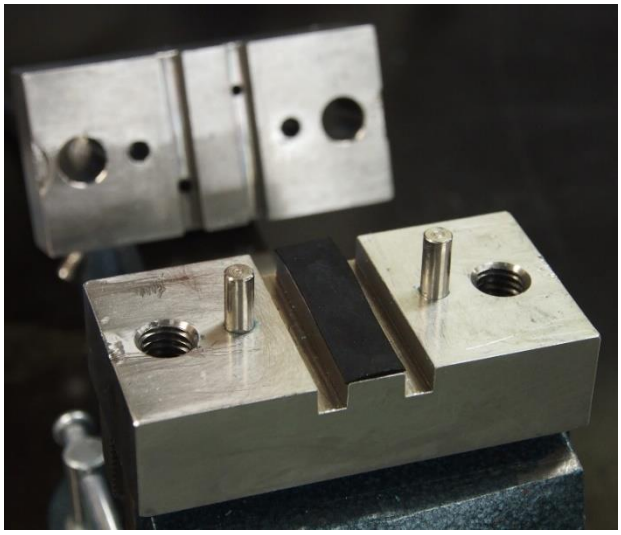

Figure 15 Permeability Measurement Setup

3.2.5. Electrical Conductivity

In-plane conductivity was measured using the Van der Pauw method [56]. A custom-made sample holder was used, and incorporated into the experimental set up as shown in Figure 16. A sample with diameter of 0.5" was placed on top of the base, with its edges touching the copper rods which created four contact points. A power supply was used to supply a current at one edge, for example between point 1 and 2. A voltmeter was connected at 3 and 4 to measure the voltage

drop. Resistivity was calculated with the following relationship.

$$R_{12,34} = \frac{V_{34}}{I_{12}} \quad \textbf{(7)}$$

The measurement was repeated for the other direction. The sheet resistance, R_s, can then be calculated by finding the value of R_s that satisfies this following equation:

$$e^{-\frac{\pi R_{12,34}}{R_s}} + e^{-\frac{\pi R_{23,41}}{R_s}} = 1 \quad \textbf{(8)}$$

The bulk conductivity, σ_{bulk}, can then be calculated using

$$\sigma_{bulk} = \frac{1}{R_s t} \quad \textbf{(9)}$$

where t is the average thickness of the sample.

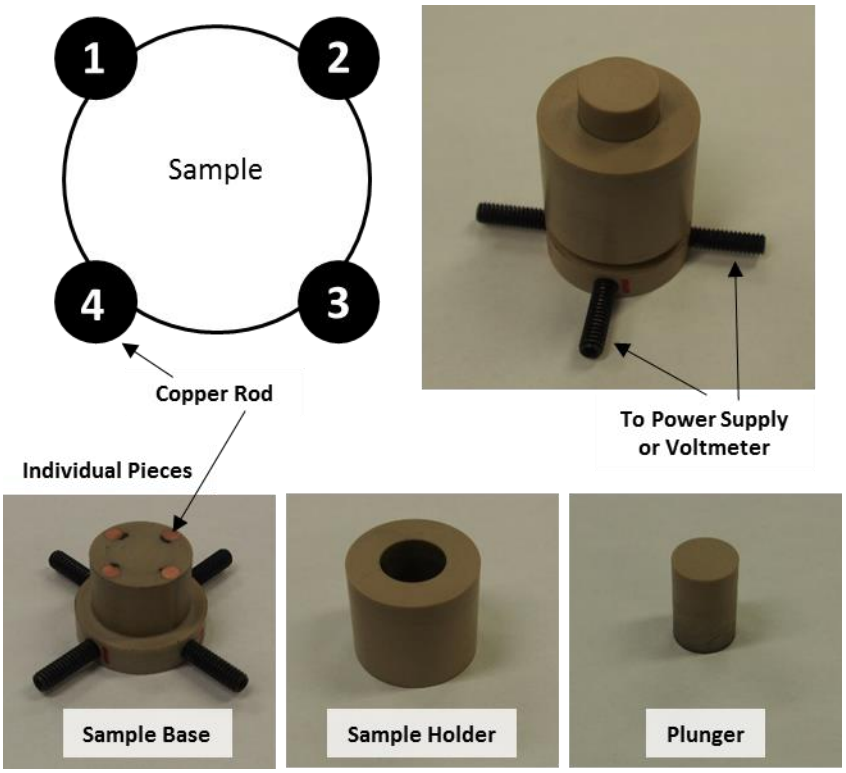

Figure 16 Conductivity sample diagram.

4. Results and Analysis

4.1. Impact of PAN Concentration and Carbonization

One of the main objectives of this work was to produce fibrous electrodes with enhanced surface area by electrospinning mats with fibers much smaller than typical GDL materials, while avoid making fibers that were too small, as these would have poor flow characteristics. Computational modeling work has previously suggested a target fiber diameter [18] around 1-2 μm. This is about 10 times lower than conventional GDL materials but about 3 times higher than typical electrospun materials [16], [49]. One of the first challenges to address was how to electrospin fibers in this intermediate size range. It is known that polymer concentration plays a major role in the fiber diameter of electrospun mats [55], with higher concentrations leading to thicker fibers. In order to produce the thickest possible fibers, the polymer concentration was increased to the highest values that could be spun without difficulty. Concentrations between 10 and 13 wt% were considered and basic analysis on both as-spun and carbonized mats were performed. A summary of the properties is presented in Table 1. SEM images of the electrospun mat before and after carbonization for the varying polymer concentration can be seen in Figure 17.

Table 1: Summary of material properties

	PAN wt%	Porosity	Fiber Diameter [um]	Electrical Conductivity [S/m]	Thickness [um]	Specific Surface Area [m^2/g]
Electrospun	10	94.67 ±0.54	0.70 ±0.30	---	758 ±233	---
	11	94.74 ±0.66	0.94 ±0.13	---	741 ±282	---
	12	93.47 ±1.28	1.14 ±0.19	---	770 ±374	---
	13	91.99 ±1.38	1.39 ±0.30	---	604 ±315	---
Carbonized	10	88.65 ±2.14	0.50 ±0.17	1519	227 ±41	---
	11	90.42 ±1.72	0.56 ±0.10	---	249 ±93	---
	12	89.10 ±2.13	0.76 ±0.18	1280 ±176	281 ±121	2.94
	13	85.30	1.22 ±0.64	---	255 ±52	---

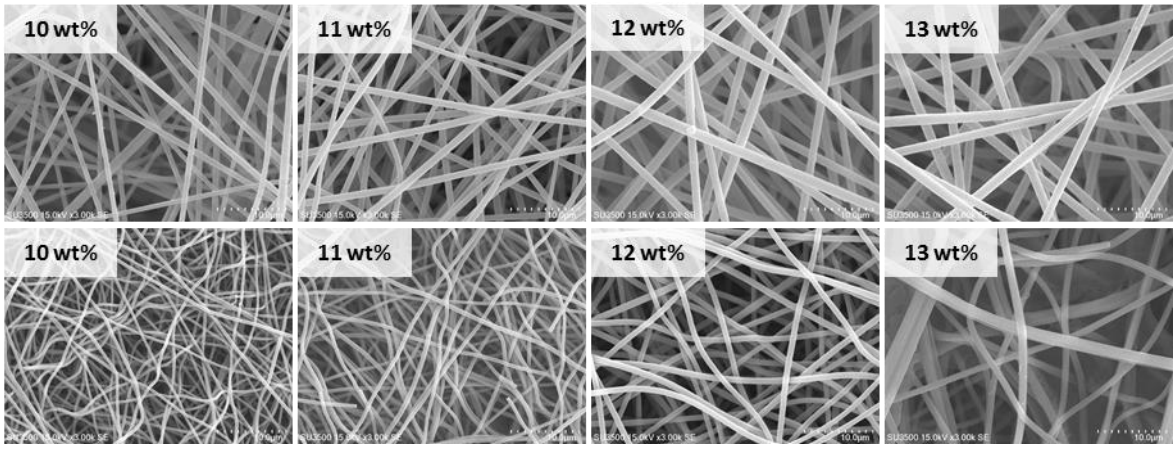

Figure 17 SEM images of electrospun samples on the top, and carbonized samples in the row below. All images are taken with magnification of 3000, and the scale bar is 10 µm.

Fiber diameter was measured for electrospun and carbonized mats and the results are shown in Figure 18(left). For each sample, 30-50 fiber diameter measurements were taken. More samples were produced and measured for the 12 wt% (5 separate samples) whereas, there were 2 sample of the 10 and 13 wt%. As expected, fiber diameter, d_f, increases with higher polymer

concentration. The d_f ranges from an average of 0.7 µm with 10 wt% to 1.4 µm with 13 wt%. During the carbonization step, the linear chains of PAN aromatize [53]. As molecules are lost in the carbonization process, the macrostructure of the electrospun mat decreases as shown in Figure 19. The weight of a mat typically decreases by about 50% after carbonization, and the thickness shrinks by about 20% to 30%. Because of this mass loss, the fiber diameter was expected to decrease after carbonization and this was observed in the SEM image analysis. For carbonized mats, d_f ranges from an average of 500 nm with 10 wt% to 1200 nm with 13 wt%. A calculation of fiber volumes per unit length based on these diameters reveals that indeed the values before and after correspond to about a 50% reduction in solid volume. The skeletal density of the carbonized materials is 1.73 g/mL on average, ranges from 1.55 g/mL to 2.14 g/mL.

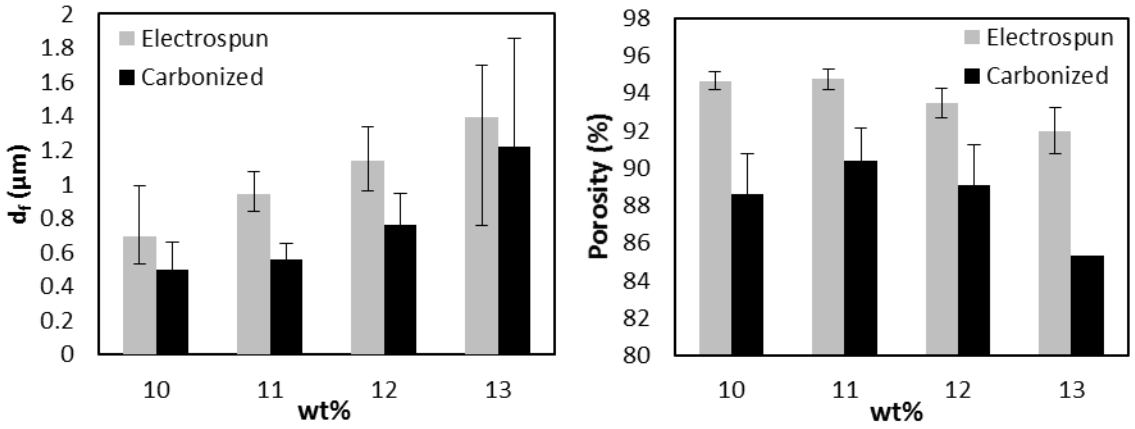

Figure 18 Effect of polymer concentration on fiber diameter and porosity.

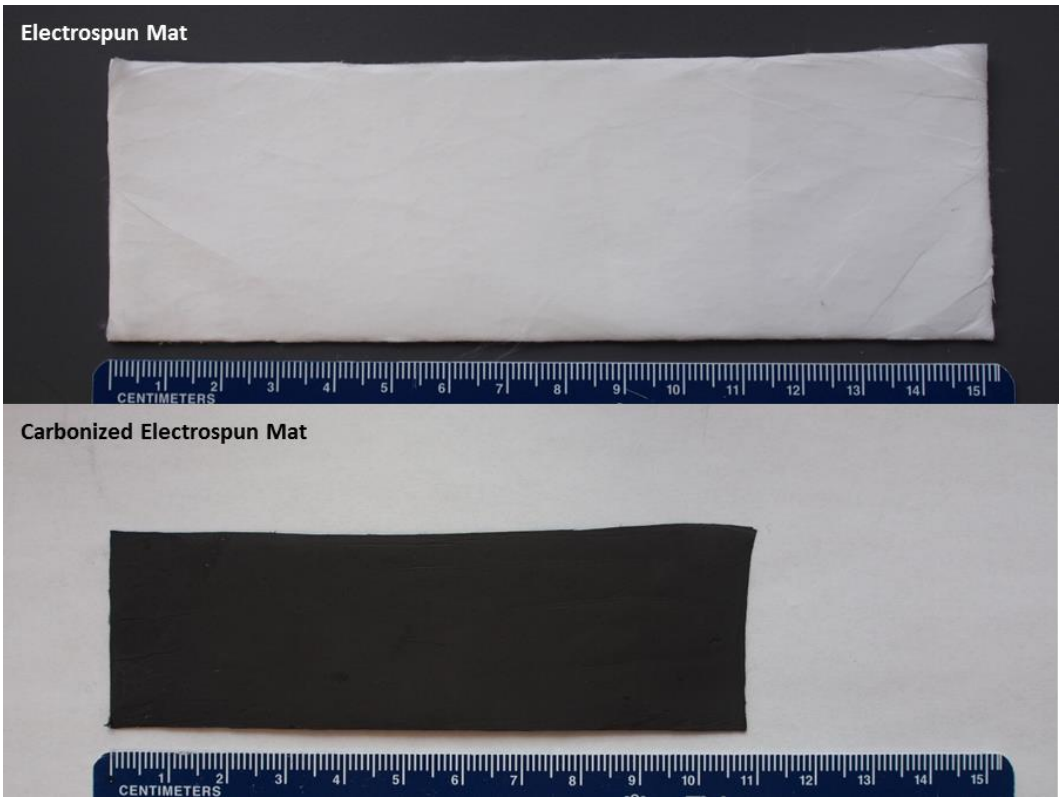

Figure 19 Images of electrospun PAN mat before and after carbonization

One of the ways to increase the permeability of a material with small fibers is to increase the porosity, as outlined in Eq. (5). Electrospinning is known to create very high porosity materials, with values typically above 90% hence its appeal for this investigation. The measured porosity of the present electrospun mats was high, ranging from 96.6% to 92% from 10 wt% to 13 wt% Figure 18 (right). The porosity decreases slightly with increasing polymer concentration, possibly because heavier fibers settle into a tighter mat during electrospinning. Upon carbonization, the porosity decreased by about 5% in absolute terms. This drop could be largely attributed to the fact that the mats are constrained between two alumina plates when placed into the furnace which means they are held in a compressed state during carbonization. Nonetheless, the porosity of carbonized mats was quite high, well within the ranges suggested by the previous modeling

[18] and much higher than typical GDL materials [19].

Overall the 12 wt% was deemed as the most suitable for the production of electrospun electrodes. Polymer concentration higher than 12 wt% produced spinning solution that was too viscous, making the electrospinning process unstable and leading to the formation of large fiber bundles in the finished product. When carbonized the 12 wt% mats have an average fiber diameter of 765 nm with 89% porosity, which is close to the target values suggested by Kok et al [18] for peak cell performance.

4.2. Detailed Characterization of Target Material (12wt%)

In the previous section, it was demonstrated that the optimal PAN concentration was 12 wt%, as this created reasonably large fibers with high porosity, while still being manageable for production. In this section, this specific material is analyzed in greater detail to characterize all the relevant physical, structural, and transport properties. Additionally, the characterization tests are applied to the material before and after carbonization to evaluate the impact of the carbonization process on the structure.

4.2.1. Specific Surface Area

Surface area was measured using the BET method. Two samples were taken, and an average surface area of the electrospun electrode was found to be 2.94 m2/g. When adjusted by the bulk density of these materials, the average specific area is 504,809 m2/m3. The theoretical specific surface area, derived from the filament analogue model using the porosity and fiber diameter were calculated and compared in

Table 2. The match between the BET measurement and the filament analogues is quite good, with only 10 to 20% error. The is a useful result as it means the filament analogue model is suitable for most first order approximations of surface area estimate, such as in numerical models of cell operation.

Table 2 : Summary of Specific Area Calculations

	EE (1)	EE (2)	SGL 25AA	Toray 90	Freudenberg
porosity [%]	0.884	0.906	0.884	0.745	0.687
df [μm]	0.87	0.87	7.33	7.72	10
Bulk Density (g/cm3)	0.196	0.154	0.202	0.478	0.54
BET A_s [m2/g]	2.4472	3.4409	1.2949	0.2172	---
BET A_s [m2/m3]	479651.2	529898.6	261569.8	103821.6	---
FA A_s [m2/m3]	533333.3	432183.9	63301.5	132124.4	125200.0
% difference from FA	-10.1	22.6	313.2	-21.4	---

The measured surface area for SGL 25AA and Toray 90, two typical electrode materials, were found to be 1.29 m^2/g and 0.2172 m^2/g. The specific surface area for the electrospun electrodes are indeed higher than these typical electrode materials, meaning that the electrospun materials were successful in terms of increasing the surface area. It is interesting that the filament analogue model predicts the surface area of the Toray 090 material fairly well, but fails to predict the surface area of SGL25AA, giving a value 3 times lower than the measured value. When looking at SEM images of Toray 090 and SGL25AA as shown in Figure 20, a significant amount of particulate material can be seen coating the fibers of the SGL material. This particulate is known as binder, and it is a polymer added to the precursor fiber structures prior to carbonization, and is also carbonized. The binder seems to increase the measured surface area substantially, which is not accounted for by the simple filament analogue model. It is difficult to

accurately gauge the electrochemically active surface area present inside the binder porosity. It is therefore difficult to compare the surface area of the made electrospun material to commercially available materials with binders. Understanding the contribution of the binder region to flow battery performance is beyond the scope of the present thesis.

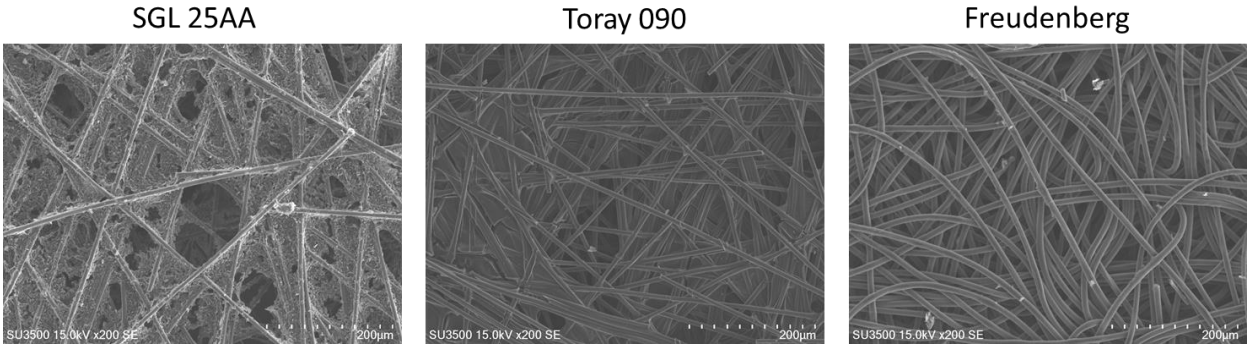

Figure 20 SEM Images of commercially available GDLs

4.2.2. Electrical Conductivity

The electrical conductivity in the in-plane direction of the 12 wt% electrospun electrodes was found to be 1280 (±176) S/m. Using the same set up, the conductivity of SGL 25AA and Toray 90 was 3,810 S/m and 16,900 S/m respectively. These two values agree with values reported in the literature, which proves the validity of the conductivity test [57], [58]. The conductivity of the electrospun mat is slightly lower than the commonly used GDLs, but are within the same order of magnitude and well above the conductivity of the electrolyte solutions which means the resistance to electron transport will be an insignificant portion of the total Ohmic polarization. The lower conductivity of the electrospun material is also expected based on the higher porosity, and hence lower solid volume fraction present to carry electric charge. Increasing the final carbonization temperature have been shown to increase the conductivity of carbonized PAN [59],

so this could be explored if higher values are sought.

4.2.3. Permeability Coefficient

In plane permeability as a function of compression was measured before and after carbonization. As expected, permeability decreased with increasing compression, since porosity and open space for flow is reduced. This trend was observed for both electrospun and carbonized materials as seen in Figure 21. Samples were taken at 2 directions perpendicular on the mat to determine the extent of anisotropy in the material. The permeability behavior for both directions are similar, and therefore the material is treated as isotropic.

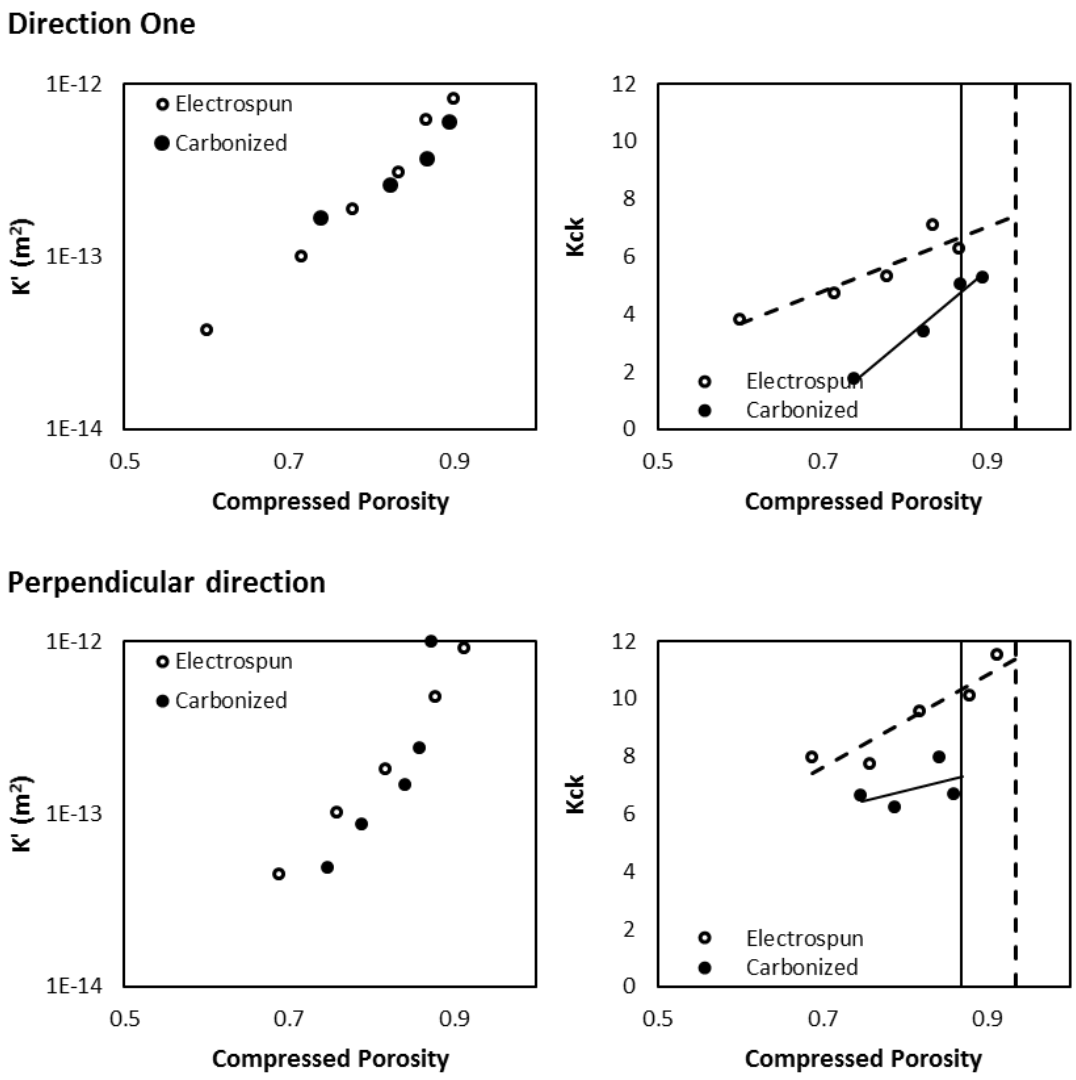

Figure 21 In-plane permeability comparison for electrospun and carbonized mats. The top row and the bottom row are experiments done on samples with orthogonal direction from the same sheet of material. The effect of compression on permeability is the on the left, and the effect of compression on k_{ck} is on the right. The vertical lines in the right graphs are the uncompressed porosities.

At first glance, the permeability, K', behaves very similarly before and after carbonization. For example, at about 80% compressed porosity, both electrospun and carbonized mat have a permeability constant of around 2×10^{-13} m^2. This implies that despite the changes to porosity and fiber diameter that have occurred during carbonization, the permeability of the material did not change significantly. Based on the Carmen-Kozeny relationship given in Eq.(5), fiber diameter,

porosity and k_{ck} all contribute to the permeability, so it is rather unexpected that the permeability remained constant. The best explanation for this is that the morphology of the fibers and their structure changed during carbonization, which would be accounted for a by a change in the Carman-Kozeny constant, k_{ck}.

From the measured porosity and fiber diameter of the electrospun and carbonized mats, the k_{ck} was calculated. As seen in Figure 21 the k_{ck} was not constant with compression, which was seen previously [17] for electrospun mats. It was attributed to non-uniform distribution of strain within the sample during compression, resulting in a high porosity (high permeability) region in the center of the sample and a lower porosity (low permeability) region near the surfaces where the sample holder was contacting the sample. This behavior of changing k_{ck} was observed to be true also for the carbonized mat. Another reason that could explain this decrease in k_{ck} with compression could be caused by a change in the structure or morphology due to fiber deformation or breakage. As seen in Figure 22, SEM images are taken of electrospun and carbonized material, before and after compression. For an electrospun material, fibers appeared to be deformed after compression. This means that more fibers are in contact with each other, closing off pores, and some have changed from cylinders to a flattened ribbon. For the carbonized material many fibers appear broken, which might cause permeability to increase due to more pathways.

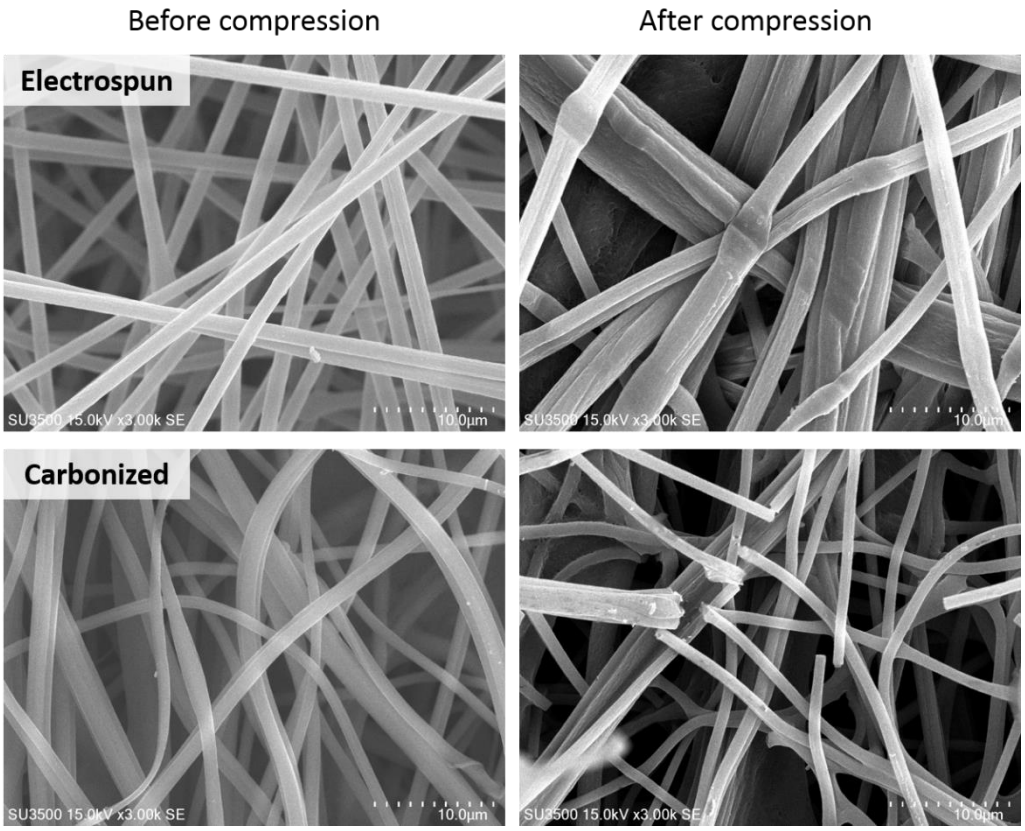

Figure 22 Effect of compression on fiber morphology for electrospun (top two images) and carbonized samples. All images are of sample made with the same 13 wt% concentration spinning solution.

It has been proposed [17] that a representative value of k_{ck} can be obtained by extrapolating back to the uncompressed porosity of the material. Following this procedure, the average projected k_{ck} of the electrospun mat was around 10, and that of carbonized mats was around 6. This decrease in k_{ck} indicates the change in structure during the carbonization step. A lower k_{ck} indicates a more permeable structure, which allowed for the fiber diameter and porosity to decrease but not causing an effect on the overall permeability. The measured k_{ck} here is higher than that reported previously, where the in-plane permeability of electrospun material was measured [17]. k_{ck} of 2 was reported for the randomly aligned mat. This increase in k_{ck} can be

attributed to the increase in fiber diameter from around 300 nm to around 1100 nm. The measured k_{ck} in this study is higher than the theoretical values of around 4.5 proposed by Tomadakis and Robertson [15]. These deviations from theoretical values could be attributed to the comparison of fibers at different scales, though the values are still very similar to theoretical values.

4.3. Characterization of Aligned Material

Material with aligned fibers have shown to increase permeability in the direction of fiber alignment [17]. Electrodes with aligned fibers are of interest in the application of flow batteries due to its increased permeability in one direction. Cell assembly can be designed to take advantage of this increase in permeability. Continuing the work done previously by Matt Kok, electrospun mats with aligned fibers was produced, by increasing the spinning speed of the collector.

The material was made with 12wt% PAN solution. All conditions were the same as the non-aligned materials. The collector was rotating at 10m/s. During carbonization, two sets of samples were prepared, one with the alignment of the fibers perpendicular to the flow of the inert gas, another that's parallel. The SEM images of carbonized sample shown in Figure 23 was produced with gas flow perpendicular to the alignment of the fiber. The sample had almost disappeared in the tube furnace when the flow was in the alignment direction of the electrospun material. It is hypothesized that during carbonization, the PAN volatizes, and this is carried away by the inert gas. The permeability of the aligned material is much higher in the direction of alignment, that most of the material was vented out by the inert gas.

The fiber diameter decreased from 1.19 µm to 0.79 µm after carbonization. The porosity of the material decreased from 91% to 87%. Aligned material was much more difficult to produce. Due to the high rotating speed of the collector, it was observed that many fibers did not deposit onto the collector, but was sprayed around in the electrospinner. This resulted in extremely long experiment time, 30-35 hours of continuous operation. Further optimization will be required to produce aligned material more consistently.

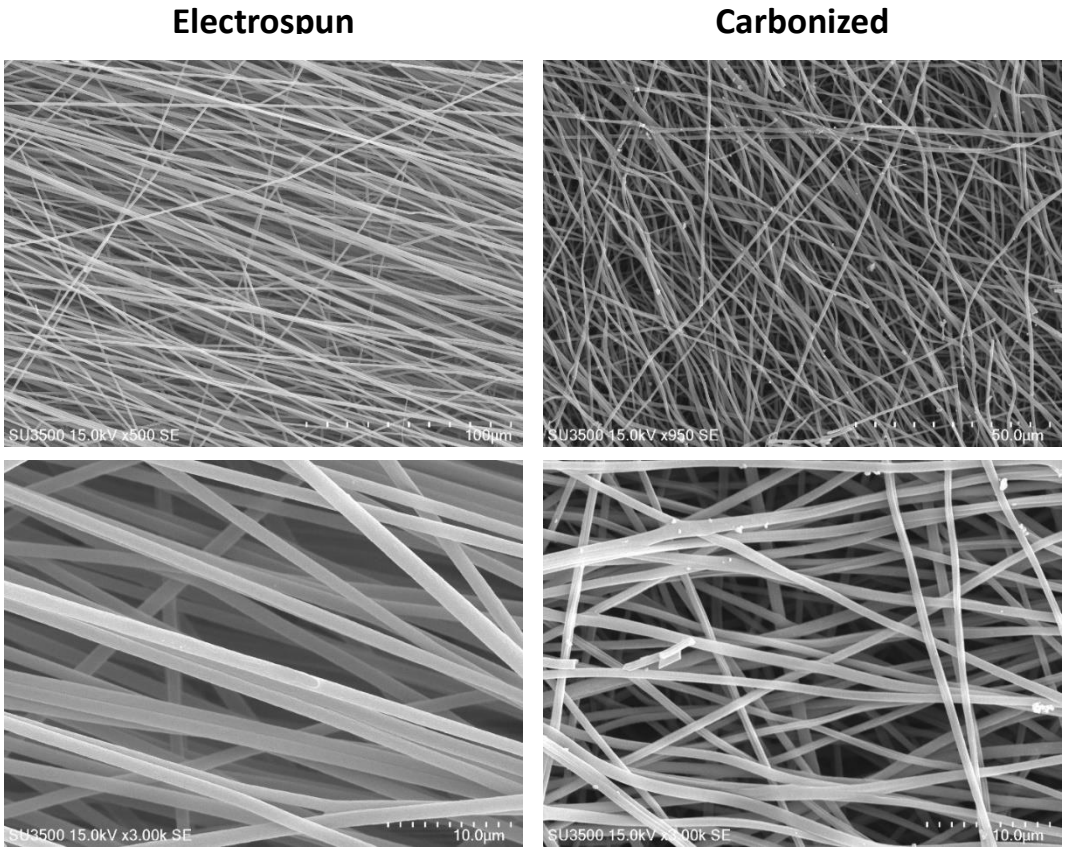

Figure 23 SEM images of aligned material, before and after carbonization

From the material created, permeability was also measured. The results are shown in Figure 24. The triangle points represent permeability data with tests done in the same direction of fiber alignment; similarly the circle open circles were tests when permeability tests were done in the perpendicular direction. As expected, permeability was higher in the same direction as the fiber alignment. It was also shown that this material had a lower k_{ck}, which was also expected.

It's important to note here, due to difficulty in reproducing these aligned fiber, these results were not tested again, and therefore, no definite conclusion can be drawn from the data, merely a proof of concept that requires further investigation.

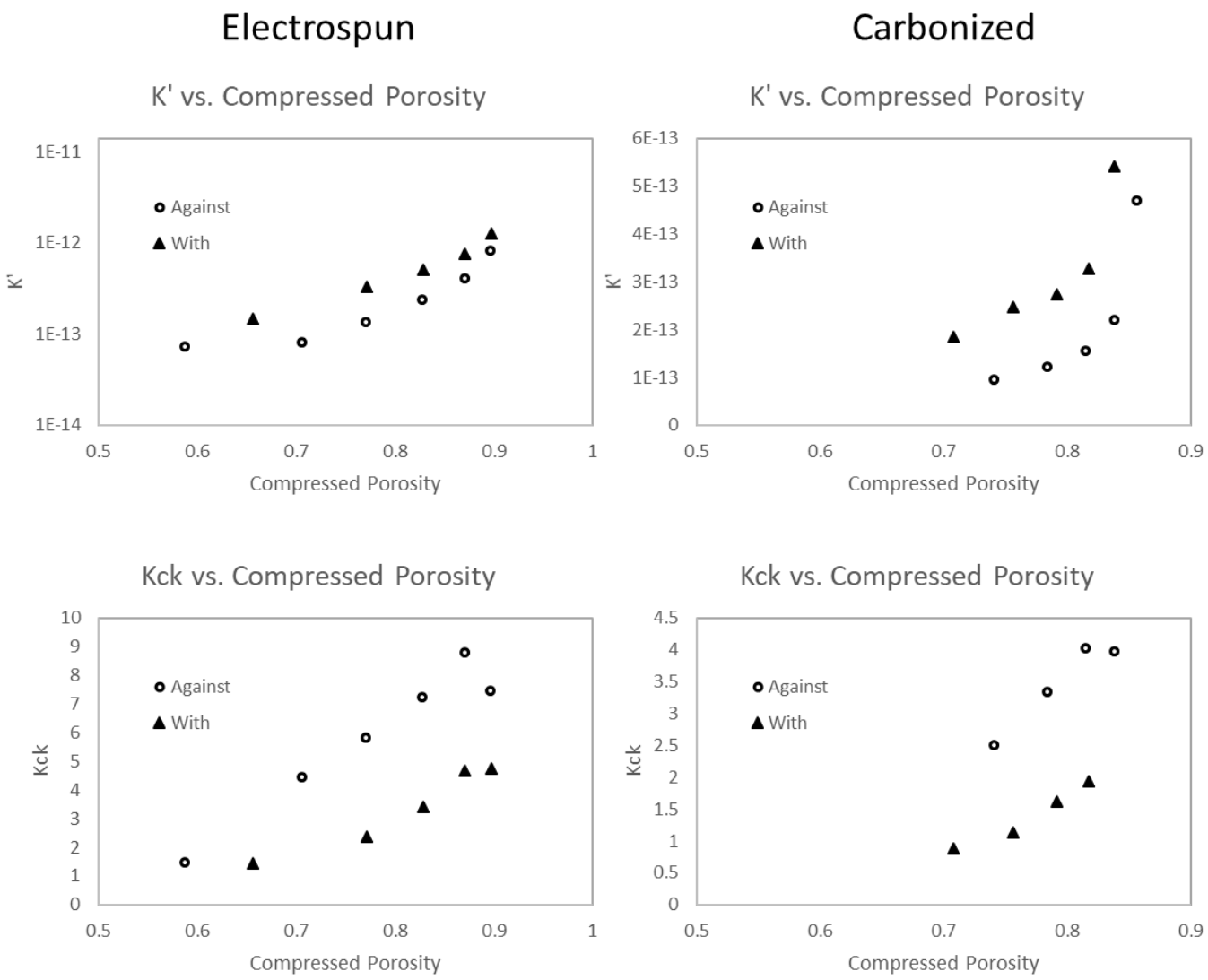

Figure 24 Permeability Data for Aligned material before and after carbonization

5. Lessons Learnt

This section highlights and summarizes the lessons learnt during this thesis. They range from material fabrication methods to further understanding and characterization of the novel material made.

DMF needs to be stored properly. The "freshness" of DMF greatly influenced how stable the electrospinning process will be. Specifically, DMF is hygroscopic and tends to adsorb water vapor from the air. This had a major detrimental impact on the stability of the electrospinning process. The power supply had to be shut off periodically to clean the needle and fiber size was not as consistent.

Polarity of the electrospinning set up effects the spinning behavior and the fiber diameter. Typically, electrospinning set up consists of the needle, charged with a high positive voltage. During our experiments, it was found that the needle can also be charged with a negative voltage. In addition, rather than charging the needle, the collector can be charged with a positive or negative voltage. It was found that charging the collector with a negative charge produced more stable spinning conditions and resulted in larger fibers. This has been studied in the literature, but the charged needle set up is the more typically used. It's hypothesized that researchers don't use a charged collector set up because it's more difficult to build, and it's not necessary for producing thin materials.

Carbonization of electrospun material decreased the total volume and fiber diameter, which was expected, as the material underwent chemical changes. Ceramic plates were used to hold the electrospun material during carbonization. This produced a smooth surface on the

outside of the final material. The ceramic plate material need to withstand high temperatures. An initial selection of material had a threshold of 1100 °C while the carbonization process goes up to 1050 °C. Material would bow after several uses. Finally, a ceramic plate with a thermal threshold of 1600 °C was used successfully.

Permeability of carbonized mats had similar trends and values compared to that of electrospun mats. This was surprising since many properties changed during carbonization. This similarity can be explained by the increase in k_{ck} during the carbonization process. This can be best explained by the change in structure during carbonization. The structure became more permeable possibly caused by the burning and removal of small fibers, melding of fibers and the creation of channels within the material. Permeability of carbonized mats increased with increasing compression, which was partially caused by fiber breaking as observed by SEM images.

6. Future Work

Now that significant amount of material can be produced, the next immediate step is to test the material in a flow battery cell. This work is being done right now with collaborators at another institution. Testing the material in an actual cell poses a new set of challenges that will require further optimization. For example, the variation in the thickness of the carbonized material creates varied compressions throughout the material when the cell is assembled and pressure is applied to the electrode. The results from these experiments will ultimately drive further optimization to prototype material that will result in higher performance.

The modeling work done by Matt Kok [18] concluded that fiber diameter between and 1 and 2 μm are desirable for an electrode for a hydrogen bromine flow battery. This study produced material with fiber meter up to 900 μm, which is still outside the desired range. Even though material with larger fibers were produced, it was not reproducible, and was therefore not further characterized. The fiber diameter can be increased by further tinkering with the electrospinning or other strategies for reduce shrinkage during the carbonization step.

As a continuation of previous work on aligned fibers done by Matt Kok [17], aligned materials, both electrospun and carbonized, were produced. The material shrunk dramatically during the carbonization step, much smaller than the permeability sample holder. Therefore, the characterization results are not complete, and further material production characterization and testing will be required. It's hypothesized that when the alignment of the fiber is in the same direction as the gas flow, the gas carries majority of material away during carbonization, and not much was left.

New microscopy technologies, X-ray tomography, have surfaced that allows us to take 3-D images of these materials. Previously, the resolution of available technologies was either too coarse or too fine. Currently, in the study, scanning electron microscope is the only imaging technique used. This is limited to what can captured on the surface of the material, and not what's underneath. The 3-D images will shed light on the consistency of the material. For example, is the fiber diameter and porosity consistent throughout the thickness of the material. In addition, these images provide another method to calculate and model the material characteristics discussed in this work. For example, by modelling flow past the fibers, permeability can be modelled and compared with experimental results. These images will help in identifying issues in our material and opportunities to improve.

Lastly, these carbonized electrospun material can be tested in other electrochemical applications, including supercapacitor electrodes or novel fuel cell gas diffusion layers. Compared to the commercially available carbon paper, which are typically used, the smaller fiber diameter and higher porosity could lead to higher performance. It would be a great opportunity to find collaborators with the testing abilities to verify the feasibility of the material.

7. Conclusion

Custom-made fibrous materials for flow battery electrode were produced with the aim of increasing reactive surface area and thereby improving cell efficiency and performance. Material properties were targeted based on previous modeling work, which suggested that fibers sizes around 1 μm and porosities above 0.85 could provide a several-fold boost in cell performance. These parameters are significantly different that the current 'off-the-shelf' materials which have 10 μm fibers, and 0.75 porosity. Electrospinning was used to make the targeted materials since this technique requires very little sophisticated equipment or tooling. One challenge was to produce fibers that were large enough, since most electrospinning research targets fibers as small as possible (100 – 300 nm). It is known that spinning higher concentrations of polymer solutions produces larger fibers. Polyacrylonitrile was electrospun in various weight-percent solutions, as concentrated as possible, in an attempt to make fibers with a diameter on the order of 1-2 μm. A concentration of 12 wt% was the upper limit since it had a low enough viscosity to be easily and stably produced, while higher concentrations were difficult to work with. The materials were carbonized using procedures widely reported in the literature, with no significant challenges. The structural and transport properties of the materials before and after carbonization were extensively studied, using a suite of experimental tools developed for fuel cell gas diffusion layers. The 12 wt% material had the desired properties, with 3x more surface area than commercially available electrodes, yet maintained a reasonable permeability due to its much higher porosity. The absolute permeability of the electrospun materials and the carbonized materials showed similar values which was surprising since a significant change in fiber size and porosity occurred

during carbonization. This suggests that the structure of the material transformed during carbonization, possible by burning and removal of small fibers, melding of some fibers and the creation of tunnels within the material. Due to the high porosity (and low solid volume fraction) of the electrospun materials, its electrical conductivity was much lower than commercially available electrodes but still far higher than the electrolyte conductivity.

Overall, this work demonstrated the feasibility of producing electrospun material for flow battery electrode via electrospinning. Future work will focus on *in-situ* testing of the materials in a flow battery. The extensive characterization and in-depth understanding of material properties will be important in further optimizing high-performance electrode for flow batteries.

8. Reference

[1] REN21, “RENEWABLES 2016 GLOBAL STATUS REPORT 2016.” REN21, 2016.

[2] P. Alotto, M. Guarnieri, and F. Moro, “Redox flow batteries for the storage of renewable energy: A review,” *Renew. Sustain. Energy Rev.*, vol. 29, pp. 325–335, Jan. 2014.

[3] T. Kousksou, P. Bruel, A. Jamil, T. El Rhafiki, and Y. Zeraouli, “Energy storage: Applications and challenges,” *Sol. Energy Mater. Sol. Cells*, vol. 120, Part A, pp. 59–80, Jan. 2014.

[4] A. Z. Weber, M. M. Mench, J. P. Meyers, P. N. Ross, J. T. Gostick, and Q. Liu, “Redox flow batteries: a review,” *J. Appl. Electrochem.*, vol. 41, no. 10, pp. 1137–1164, Sep. 2011.

[5] B. Huskinson *et al.*, “A metal-free organic-inorganic aqueous flow battery,” *Nature*, vol. 505, no. 7482, pp. 195–198, Jan. 2014.

[6] L. Su, J. A. Kowalski, K. J. Carroll, and F. R. Brushett, “Recent Developments and Trends in Redox Flow Batteries,” in *Rechargeable Batteries*, Z. Zhang and S. S. Zhang, Eds. Springer International Publishing, 2015, pp. 673–712.

[7] R. M. Darling and M. L. Perry, “The Influence of Electrode and Channel Configurations on Flow Battery Performance,” *J. Electrochem. Soc.*, vol. 161, no. 9, pp. A1381–A1387, Jan. 2014.

[8] D. S. Aaron *et al.*, “Dramatic performance gains in vanadium redox flow batteries through modified cell architecture,” *J. Power Sources*, vol. 206, pp. 450–453, May 2012.

[9] K. T. Cho, P. Ridgway, A. Z. Weber, S. Haussener, V. Battaglia, and V. Srinivasan, “High Performance Hydrogen/Bromine Redox Flow Battery for Grid-Scale Energy Storage,” *J. Electrochem. Soc.*, vol. 159, no. 11, pp. A1806–A1815, Jan. 2012.

[10] M. C. Tucker, K. T. Cho, A. Z. Weber, G. Lin, and T. V. Nguyen, “Optimization of electrode characteristics for the Br2/H2 redox flow cell,” *J. Appl. Electrochem.*, vol. 45, no. 1, pp. 11–19, Oct. 2014.

[11] I. Mayrhuber, C. R. Dennison, V. Kalra, and E. C. Kumbur, “Laser-perforated carbon paper electrodes for improved mass-transport in high power density vanadium redox flow batteries,” *J. Power Sources*, vol. 260, pp. 251–258, Aug. 2014.

[12] G. Lin *et al.*, “Advanced Hydrogen-Bromine Flow Batteries with Improved Efficiency, Durability and Cost,” *J. Electrochem. Soc.*, vol. 163, no. 1, pp. A5049–A5056, Jan. 2016.

[13] V. Yarlagadda, G. Lin, P. Y. Chong, and T. V. Nguyen, “High Surface Area Carbon Electrodes for Bromine Reactions in H2-Br2 Fuel Cells,” *J. Electrochem. Soc.*, vol. 163, no. 1, pp. A5126–A5133, Jan. 2016.

[14] A. M. Pezeshki, J. T. Clement, G. M. Veith, T. A. Zawodzinski, and M. M. Mench, “High performance electrodes in vanadium redox flow batteries through oxygen-enriched thermal activation,” *J. Power Sources*, vol. 294, pp. 333–338, Oct. 2015.

[15] M. M. Tomadakis and T. J. Robertson, “Viscous Permeability of Random Fiber Structures: Comparison of Electrical and Diffusional Estimates with Experimental and Analytical Results,” *J. Compos. Mater.*, vol. 39, no. 2, pp. 163–188, Jan. 2005.

[16] J. T. Gostick, M. W. Fowler, M. D. Pritzker, M. A. Ioannidis, and L. M. Behra, “In-plane and through-plane gas permeability of carbon fiber electrode backing layers,” *J. Power Sources*, vol. 162, no. 1, pp. 228–238, Nov. 2006.

[17] M. D. R. Kok and J. T. Gostick, “Transport properties of electrospun fibrous membranes

with controlled anisotropy," *J. Membr. Sci.*, vol. 473, pp. 237–244, Jan. 2015.
[18] M. D. R. Kok, A. Khalifa, and J. T. Gostick, "Multiphysics Simulation of the Flow Battery Cathode: Cell Architecture and Electrode Optimization," *J. Electrochem. Soc.*, vol. 163, no. 7, pp. A1408–A1419, Jan. 2016.
[19] R. R. Rashapov, J. Unno, and J. T. Gostick, "Characterization of PEMFC Gas Diffusion Layer Porosity," *J. Electrochem. Soc.*, vol. 162, no. 6, pp. F603–F612, Jan. 2015.
[20] Z.-M. Huang, Y.-Z. Zhang, M. Kotaki, and S. Ramakrishna, "A review on polymer nanofibers by electrospinning and their applications in nanocomposites," *Compos. Sci. Technol.*, vol. 63, no. 15, pp. 2223–2253, Nov. 2003.
[21] E. Frank, L. M. Steudle, D. Ingildeev, J. M. Spörl, and M. R. Buchmeiser, "Carbon Fibers: Precursor Systems, Processing, Structure, and Properties," *Angew. Chem. Int. Ed.*, vol. 53, no. 21, pp. 5262–5298, May 2014.
[22] T. Wang and S. Kumar, "Electrospinning of polyacrylonitrile nanofibers," *J. Appl. Polym. Sci.*, vol. 102, no. 2, pp. 1023–1029, Oct. 2006.
[23] L. Zhang, A. Aboagye, A. Kelkar, C. Lai, and H. Fong, "A review: carbon nanofibers from electrospun polyacrylonitrile and their applications," *J. Mater. Sci.*, vol. 49, no. 2, pp. 463–480, Sep. 2013.
[24] E. Fitzer, W. Frohs, and M. Heine, "Optimization of stabilization and carbonization treatment of PAN fibres and structural characterization of the resulting carbon fibres," *Carbon*, vol. 24, no. 4, pp. 387–395, Jan. 1986.
[25] E. Zussman *et al.*, "Mechanical and structural characterization of electrospun PAN-derived carbon nanofibers," *Carbon*, vol. 43, no. 10, pp. 2175–2185, Aug. 2005.
[26] S. Y. Gu, J. Ren, and Q. L. Wu, "Preparation and structures of electrospun PAN nanofibers as a precursor of carbon nanofibers," *Synth. Met.*, vol. 155, no. 1, pp. 157–161, Oct. 2005.
[27] Y. Yang, F. Simeon, T. A. Hatton, and G. C. Rutledge, "Polyacrylonitrile-based electrospun carbon paper for electrode applications," *J. Appl. Polym. Sci.*, vol. 124, no. 5, pp. 3861–3870, Jun. 2012.
[28] X. Mao, T. A. Hatton, and G. C. Rutledge, "A Review of Electrospun Carbon Fibers as Electrode Materials for Energy Storage," *Curr. Org. Chem.*, vol. 17, no. 13, pp. 1390–1401, Jul. 2013.
[29] B. Zhang, F. Kang, J.-M. Tarascon, and J.-K. Kim, "Recent advances in electrospun carbon nanofibers and their application in electrochemical energy storage," *Prog. Mater. Sci.*, vol. 76, pp. 319–380, Mar. 2016.
[30] S. Peng *et al.*, "Electrospun carbon nanofibers and their hybrid composites as advanced materials for energy conversion and storage," *Nano Energy*, vol. 22, pp. 361–395, Apr. 2016.
[31] G. Wang, L. Zhang, and J. Zhang, "A review of electrode materials for electrochemical supercapacitors," *Chem Soc Rev*, vol. 41, no. 2, pp. 797–828, 2012.
[32] D. Todd and W. Mérida, "Morphologically controlled fuel cell transport layers enabled via electrospun carbon nonwovens," *J. Power Sources*, vol. 273, pp. 312–316, Jan. 2015.
[33] G. Wei, J. Liu, H. Zhao, and C. Yan, "Electrospun carbon nanofibres as electrode materials toward VO2+/VO2+ redox couple for vanadium flow battery," *J. Power Sources*, vol. 241, pp. 709–717, Nov. 2013.

[34] A. Fetyan *et al.*, “Electrospun Carbon Nanofibers as Alternative Electrode Materials for Vanadium Redox Flow Batteries,” *ChemElectroChem*, vol. 2, no. 12, pp. 2055–2060, Dec. 2015.
[35] H. Lund and G. Salgi, “The role of compressed air energy storage (CAES) in future sustainable energy systems,” *Energy Convers. Manag.*, vol. 50, no. 5, pp. 1172–1179, May 2009.
[36] P. Sharma and T. S. Bhatti, “A review on electrochemical double-layer capacitors,” *Energy Convers. Manag.*, vol. 51, no. 12, pp. 2901–2912, Dec. 2010.
[37] V. Etacheri, R. Marom, R. Elazari, G. Salitra, and D. Aurbach, “Challenges in the development of advanced Li-ion batteries: a review,” *Energy Environ. Sci.*, vol. 4, no. 9, pp. 3243–3262, 2011.
[38] M. Skyllas-Kazacos, M. H. Chakrabarti, S. A. Hajimolana, F. S. Mjalli, and M. Saleem, “Progress in Flow Battery Research and Development,” *J. Electrochem. Soc.*, vol. 158, no. 8, pp. R55–R79, Aug. 2011.
[39] G. Kear, A. A. Shah, and F. C. Walsh, “Development of the all-vanadium redox flow battery for energy storage: a review of technological, financial and policy aspects,” *Int. J. Energy Res.*, vol. 36, no. 11, pp. 1105–1120, Sep. 2012.
[40] F. R. Brushett, J. T. Vaughey, and A. N. Jansen, “An All-Organic Non-aqueous Lithium-Ion Redox Flow Battery,” *Adv. Energy Mater.*, vol. 2, no. 11, pp. 1390–1396, Nov. 2012.
[41] M. H. Chakrabarti, E. P. L. Roberts, C. Bae, and M. Saleem, “Ruthenium based redox flow battery for solar energy storage,” *Energy Convers. Manag.*, vol. 52, no. 7, pp. 2501–2508, Jul. 2011.
[42] C. L. Casper, J. S. Stephens, N. G. Tassi, D. B. Chase, and J. F. Rabolt, “Controlling Surface Morphology of Electrospun Polystyrene Fibers: Effect of Humidity and Molecular Weight in the Electrospinning Process,” *Macromolecules*, vol. 37, no. 2, pp. 573–578, Jan. 2004.
[43] E. J. Chong *et al.*, “Evaluation of electrospun PCL/gelatin nanofibrous scaffold for wound healing and layered dermal reconstitution,” *Acta Biomater.*, vol. 3, no. 3, pp. 321–330, May 2007.
[44] B.-M. Min *et al.*, “Chitin and chitosan nanofibers: electrospinning of chitin and deacetylation of chitin nanofibers,” *Polymer*, vol. 45, no. 21, pp. 7137–7142, Sep. 2004.
[45] L. Ji, M. Rao, S. Aloni, L. Wang, E. J. Cairns, and Y. Zhang, “Porous carbon nanofiber–sulfur composite electrodes for lithium/sulfur cells,” *Energy Environ. Sci.*, vol. 4, no. 12, p. 5053, 2011.
[46] W. E. Teo and S. Ramakrishna, “A review on electrospinning design and nanofibre assemblies,” *Nanotechnology*, vol. 17, no. 14, p. R89, 2006.
[47] J. M. Deitzel, J. Kleinmeyer, D. Harris, and N. C. Beck Tan, “The effect of processing variables on the morphology of electrospun nanofibers and textiles,” *Polymer*, vol. 42, no. 1, pp. 261–272, Jan. 2001.
[48] J.-H. He, Y.-Q. Wan, and J.-Y. Yu, “Effect of concentration on electrospun polyacrylonitrile (PAN) nanofibers,” *Fibers Polym.*, vol. 9, no. 2, pp. 140–142, Apr. 2008.
[49] R. Jalili, S. A. Hosseini, and M. Morshed, “The effects of operating parameters on the morphology of electrospun polyacrilonitrile nanofibres,” *Iran. Polym. J.*, vol. 14, no. 12, p. 1074, 2005.

[50] A. l. Yarin, “Coaxial electrospinning and emulsion electrospinning of core–shell fibers,” *Polym. Adv. Technol.*, vol. 22, no. 3, pp. 310–317, Mar. 2011.
[51] X. Wang, H. Niu, X. Wang, and T. Lin, “Needleless Electrospinning of Uniform Nanofibers Using Spiral Coil Spinnerets,” *J Nanomater.*, vol. 2012, p. 3:1–3:9, Jan. 2012.
[52] A. L. Yarin and E. Zussman, “Upward needleless electrospinning of multiple nanofibers,” *Polymer*, vol. 45, no. 9, pp. 2977–2980, Apr. 2004.
[53] M. S. A. Rahaman, A. F. Ismail, and A. Mustafa, “A review of heat treatment on polyacrylonitrile fiber,” *Polym. Degrad. Stab.*, vol. 92, no. 8, pp. 1421–1432, Aug. 2007.
[54] U. Ali, X. Wang, and T. Lin, “Effect of nozzle polarity and connection on electrospinning of polyacrylonitrile nanofibers,” *J. Text. Inst.*, vol. 103, no. 11, pp. 1160–1168, Nov. 2012.
[55] S. Y. Gu, J. Ren, and G. J. Vancso, “Process optimization and empirical modeling for electrospun polyacrylonitrile (PAN) nanofiber precursor of carbon nanofibers,” *Eur. Polym. J.*, vol. 41, no. 11, pp. 2559–2568, Nov. 2005.
[56] L. J. Van der Pauw, “A Method of measuring the resistiviy and Hall Coefficient on Lamellae of Arbitrary Shape,” *Philips Tech. Rev.*, vol. 26, pp. 220–224, 1958.
[57] I. Nitta, T. Hottinen, O. Himanen, and M. Mikkola, “Inhomogeneous compression of PEMFC gas diffusion layer: Part I. Experimental,” *J. Power Sources*, vol. 171, no. 1, pp. 26–36, Sep. 2007.
[58] D. Natarajan and T. Van Nguyen, “Effect of electrode configuration and electronic conductivity on current density distribution measurements in PEM fuel cells,” *J. Power Sources*, vol. 135, no. 1–2, pp. 95–109, Sep. 2004.
[59] Z. Zhou *et al.*, “Development of carbon nanofibers from aligned electrospun polyacrylonitrile nanofiber bundles and characterization of their microstructural, electrical, and mechanical properties,” *Polymer*, vol. 50, no. 13, pp. 2999–3006, Jun. 2009.